AMERICAN SOCIETY FOR MICROBIOLOGY | Molecular and Cellular Biology

A Role of TMEM16E Carrying a Scrambling Domain in Sperm Motility

Sayuri Gyobu,[a] Haruhiko Miyata,[b] Masahito Ikawa,[b] Daiju Yamazaki,[c]* Hiroshi Takeshima,[c] Jun Suzuki,[a] Shigekazu Nagata[a]

Laboratory of Biochemistry & Immunology, Immunology Frontier Research Center,[a] and Department of Experimental Genome Research, Research Institute for Microbial Diseases,[b] Osaka University, Suita, Osaka, Japan; Department of Biological Chemistry, Graduate School of Pharmaceutical Sciences, Kyoto University, Kyoto, Japan[c]

Transmembrane protein 16E (TMEM16E) belongs to the TMEM16 family of proteins that have 10 transmembrane regions and appears to localize intracellularly. Although TMEM16E mutations cause bone fragility and muscular dystrophy in humans, its biochemical function is unknown. In the TMEM16 family, TMEM16A and -16B serve as Ca^{2+}-dependent Cl^- channels, while TMEM16C, -16D, -16F, -16G, and -16J support Ca^{2+}-dependent phospholipid scrambling. Here, we show that TMEM16E carries a segment composed of 35 amino acids homologous to the scrambling domain in TMEM16F. When the corresponding segment of TMEM16A was replaced by this 35-amino-acid segment of TMEM16E, the chimeric molecule localized to the plasma membrane and supported Ca^{2+}-dependent scrambling. We next established *TMEM16E*-deficient mice, which appeared to have normal skeletal muscle. However, fertility was decreased in the males. We found that TMEM16E was expressed in germ cells in early spermatogenesis and thereafter and localized to sperm tail. *TMEM16E*$^{-/-}$ sperm showed no apparent defect in morphology, beating, mitochondrial function, capacitation, or binding to zona pellucida. However, they showed reduced motility and inefficient fertilization of cumulus-free but zona-intact eggs *in vitro*. Our results suggest that TMEM16E may function as a phospholipid scramblase at inner membranes and that its defect affects sperm motility.

Transmembrane protein 16E (TMEM16E), also called anoctamin 5 (Ano5) or gnathodiaphyseal dysplasia 1 (GDD1), belongs to the TMEM16 family of proteins, which carry 10 transmembrane regions with cytosolic N- and C-terminal extensions (1–3). There are 10 human TMEM16 family proteins (TMEM16A to -H, -J, and -K [Ano1 to -10]). TMEM16E is highly expressed in muscle and bone (4–6). *TMEM16E* was originally identified as the causative gene for an autosomal dominant disorder, GDD, in which the cysteine residue at amino acid position 356 was mutated to glycine or arginine in two families (7). Subsequently, *TMEM16E* homozygous and compound heterozygous mutations (missense or frameshift mutations) and a dominant missense mutation were found in patients with autosomal muscular dystrophies (8–10) and GDD (11). A recent cohort analysis of 786 patients with autosomal recessive limb-girdle muscular dystrophies (LGMD) and generic myopathy found that about 4% and 3% of the patients, respectively, carried pathological homozygous or compound heterozygous *TMEM16E* mutations (12).

Despite the severe phenotypes seen in human patients with *TMEM16E* mutations, TMEM16E's biochemical and physiological functions have not been determined (13). Since TMEM16A, the first-identified TMEM16 family protein, functions as a Ca^{2+}-dependent Cl^- channel (14–16), TMEM16E was also thought to be a Cl^- channel (12). We demonstrated that TMEM16F supports Ca^{2+}-dependent phospholipid scrambling at plasma membranes (6, 17), and TMEM16F's ability to scramble phospholipids was recently confirmed by two other groups (18, 19). Furthermore, Yu et al. (18) showed that replacing a small region (35 amino acids) in mouse TMEM16A's transmembrane IV-V region (Asp554 to Lys588) with the corresponding region from TMEM16F fully conferred scramblase activity to TMEM16A. Thus, this region of TMEM16F was designated a scrambling domain (SCRD).

We previously expressed each TMEM16 family member in a *TMEM16F*-null cell line and found that not only TMEM16F but also TMEM16C, -16D, -16G, and -16J support Ca^{2+}-dependent phospholipid scrambling at plasma membranes (6). Patch-clamp analysis performed with 293T cells expressing each TMEM16 family member confirmed Cl^--channel activity only in TMEM16A and -16B. We found neither Cl^--channel nor scramblase activity in TMEM16E and concluded that this was due to its intracellular localization (7). In this study, we sought to determine the activity and physiological function of TMEM16E in mice. We first confirmed the presence of TMEM16E in the intracellular membranes of mouse skeletal muscle using a hamster monoclonal antibody (MAb) against mouse TMEM16E. We also found that a 35-amino-acid segment in the transmembrane IV-V region of TMEM16E is highly homologous to the SCRD of TMEM16F. When this segment of TMEM16E was substituted for the corresponding region of TMEM16A, the resulting chimeric molecule localized to the plasma membrane and strongly promoted phospholipid scrambling.

We next established *TMEM16E*-deficient mice. Unlike human patients with a loss-of-function *TMEM16E* mutation, *TMEM16E*$^{-/-}$ mice had no apparent skeletal muscle abnormalities. However, fertility in the males was strongly reduced by impaired sperm motility. Collectively, our findings indicate that TMEM16E may sup-

Received 3 October 2015 **Returned for modification** 19 October 2015
Accepted 7 December 2015
Accepted manuscript posted online 14 December 2015
Citation Gyobu S, Miyata H, Ikawa M, Yamazaki D, Takeshima H, Suzuki J, Nagata S. 2016. A role of TMEM16E carrying a scrambling domain in sperm motility. Mol Cell Biol 36:645–659. doi:10.1128/MCB.00919-15.

Address correspondence to Shigekazu Nagata, snagata@ifrec.osaka-u.ac.jp.
* Present address: Daiju Yamazaki, Division of Pharmacology, National Institute of Health Sciences, Tokyo, Japan.

port phospholipid scrambling at the intracellular membrane architecture and that its defect affects sperm motility.

MATERIALS AND METHODS

Mice. C57BL6/J and *W/W*^{v} mice were purchased from Japan SLC. B6D2F1 mice were purchased from CLEA Japan, and their eggs were used for *in vitro* fertilization (IVF). Mice with a conditional *TMEM16E* deletion were generated by Unitech as a custom order. Briefly, a targeting vector was designed to replace the 1.6-kb DNA fragment containing exon 2 of *TMEM16E* with a neo-loxP cassette (20). A diphtheria toxin A (*DT-A*) sequence driven by the thymidine kinase (*tk*) promoter was placed at the 5′ end of the vector. C57BL6/J ES cells (clone Bruce 4) were transfected with the targeting vector, and G418-resistant clones were screened for homologous recombination by PCR. Positive clones were injected into blastocysts from BALB/c mice, and *TMEM16E*$^{+/\mathrm{NeoFRT}}$ mice (FRT, FLP recombination target) were crossed with *CAG-CRE* mice (21) to obtain *TMEM16E*$^{+/-}$ mice.

The *TMEM16E* genotype was determined by PCR using a forward primer (5′-GGTTGTATTGGTTCTTAAATTGTGG) and two reverse primers (5′-AACCGAAGACTGTCACATGTGGAAT for the wild type and 5′-AATTCATTCTCGATTCTTGATGG for the mutant allele). All mice were housed in specific-pathogen-free facilities at the Kyoto University Graduate School of Medicine and at the Research Institute for Microbial Diseases, Osaka University. All animal experiments were conducted according to protocols approved by the Kyoto University Animal Care and Use Committee and by the Animal Research Committee of the Research Institute for Microbial Diseases, Osaka University.

Antibodies and reagents. Monoclonal antibodies against mouse TMEM16E were generated in Armenian hamsters as described previously (22). Briefly, the TMEM16E C-terminal region (amino acids 847 to 904, referred to as TMEM16E-c) was fused to glutathione *S*-transferase (GST) or maltose binding protein (MBP), synthesized in *Escherichia coli* BL21, and purified with glutathione-Sepharose (GE Healthcare) or amylose resin (New England BioLabs). The purified protein was injected subcutaneously (s.c.) into Armenian hamsters four times at 2-week intervals, and a booster injection was administered into the footpad. Lymphocytes from the immunized hamsters' popliteal and inguinal lymph nodes were fused with mouse NSO$^{\mathrm{Bcl\text{-}2}}$ myeloma (23), and hybridomas were selected in HAT medium (Dulbecco's modified Eagle's medium [DMEM] containing 10% fetal calf serum [FCS; Gibco], 10% NCTC-109 [Gibco], 1% nonessential amino acids [Gibco], 5.5 U/ml human interleukin-6 [IL-6] [provided by Ajinomoto], 100 μM hypoxanthine, 0.4 μM aminopterin, and 16 μM thymidine). Hybridomas were screened by enzyme-linked immunosorbent assay (ELISA) using MBP-fused TMEM16E-c. A positive clone was cultured in GIT medium (Nihon Pharmaceutical), and the antibodies were purified using protein A-Sepharose (GE Healthcare). Rabbit anti-mouse TMEM16F serum was as previously described (6). Mouse anti-α-tubulin MAb (clone AB-1), goat anti-mouse basigin, rabbit anticalnexin, and mouse anti-Golgin97 MAb were from Oncogene Science, Santa Cruz, ENZO Life Sciences, and Thermo Fisher Scientific, respectively. We obtained horseradish peroxidase (HRP)-conjugated goat anti-mouse Igs, goat anti-rabbit Igs, and rabbit anti-goat Igs from Dako, AffiniPure goat anti-Armenian hamster IgG from Jackson ImmunoResearch, and anti-Flag MAb (M2) from Sigma-Aldrich. Mouse IL-3 was produced as previously described (24). Rabbit anti-mouse SPACA1 antibody was described previously (25). HRP-mouse antiphosphotyrosine MAb (clone 4G10) was from Millipore.

cDNAs. Mouse cDNAs for TMEM16F (NCBI; GenBank accession no. NM_175344) and TMEM16A (GenBank accession no. BC062959.1), as well as the edited cDNA for TMEM16E (NCBI; GenBank accession no. NM_177694.5), were described previously (6). TMEM16A cDNAs carrying the SCRD of TMEM16F (amino acids 525 to 559) or TMEM16E (amino acids 521 to 555) were constructed by fusing three DNA fragments using In-Fusion HD cloning kits (TaKaRa Clontech). The authenticity of the sequences was confirmed by sequencing.

Cell lines, *TMEM16F*$^{-/-}$ Ba/F3 cells, and transformation. Mouse Ba/F3 cells were maintained in RPMI medium containing 10% FCS, 45 U/ml mouse IL-3, and 50 μM 2-mercaptoethanol. Mouse C2C12 and human 293T cells were cultured in DMEM containing 10% FCS. Plat-E cells (26) were cultured in DMEM containing 10% FCS, 10 μg/ml blasticidin S, and 1 μg/ml puromycin.

The *TMEM16F*$^{-/-}$ Ba/F3 cell line was established by the use of the clustered regularly interspersed short palindromic repeats (CRISPR)-Cas (CRISPR-associated) system (27). In brief, a pair of target DNA sequences (5′-CACCGGGATGAAGTCGATTCGCCTC and 5′-AAACGAGGCGA ATCGACTTCATCCC) were designed with the CRISPR Design Tool at Feng Zhang's laboratory (www.genome-engineering.org/crispr/?page_id =41). The annealed fragments were inserted into a BbsI-digested pX330 vector (Addgene). Ba/F3 cells (1.0×10^6) were transfected twice with 10 μg of the plasmid by electroporation using an NEPA21 system (Nepagene) (140 V, 5 ms), cultured at 37°C for 3 days, and subjected to limiting dilution. The mutated allele was identified by sequencing the DNA fragment flanking the CRISPR-Cas target site. For the transformation of *TMEM16F*$^{-/-}$ Ba/F3 cells, cDNAs were introduced into pMXs-puro c-enhanced green fluorescent protein (c-EGFP) to express a protein tagged with EGFP at the C terminus. Retroviruses were produced in Plat-E, concentrated by centrifugation as described previously (28), and used to infect *TMEM16F*$^{-/-}$ Ba/F3 cells. After repeating the infection process twice, transformants were selected in the presence of 2 μg/ml puromycin and sorted by the use of FACSAria II (BD Biosciences).

To analyze the cellular localization of EGFP-tagged TMEM16, 293T cells were transfected using Fugene 6 (Promega) with pMXs-puro carrying cDNA for the N- or C-terminally EGFP-tagged TMEM16 or its derivatives. Stable transformants, selected by culturing with 1 μg/ml puromycin, were grown on gelatin-coated glass dishes and observed by confocal microscopy (FV-1000D; Olympus).

Real-time PCR. RNA was isolated using Isogen (Nippon Gene) and an RNeasy Micro kit (Qiagen) and subjected to reverse transcription (RT) with a High Capacity RNA-to-cDNA kit (Thermo Fisher Scientific). An aliquot of the product was amplified in a mixture containing LightCycler 480 SYBR green I Master (Roche Diagnostics) according to the manufacturer's instructions. We used the following primers: for *TMEM16A*, 5′-ACCCCGACGCCGAATGCAAG and 5′-GCTGGTCCTG CCTGACGCTG; for *TMEM16B*, 5′-GAGGCGCACACCTGGGTCAC and 5′-ATGGGGCGTGGATCCGGACA; for *TMEM16C*, 5′-GCCAG-CAATTGCCAACCCCG and 5′-GCAGTCCGACTCCTCCAGCTCT; for *TMEM16D*, 5′-ACAGGCATGCTCTTCCCCGC and 5′-GCGATCACTG CTCGGCGTCT; for *TMEM16E*, 5′-AGCAGCTCCAGCTTCGGCCT and 5′-TTCACGCTCTGCAGGGTGGC; for *TMEM16F*, 5′-GCGCCAG GCAGAGCTCGAAT and 5′-AGAAGACGGCGCTCGCACAC; for *TMEM16G*, 5′-ACATGTGCCCGCTGTGCTCC and 5′-GGGCCGAGG CCTCTCCTCAA; for *TMEM16H*, 5′-TGGAGGAGCCACGTCCCCAG and 5′-GCGGGGCAGACCCTTCACAC; for *TMEM16J*, 5′-GCTGTGGT GGTGACTGGGGC and 5′-CCAGGCGCGTGGATTTCCCA; for *TMEM16K*, 5′-TGGGGGCAGAAGCAGTCGGT and 5′-GGCCTGTGG GTAGCCAGGGAT; and for GAPDH (glyceraldehyde-3-phosphate dehydrogenase), 5′-ATGGTGAAGGTCGGTGAA and 5′-TTACTCCTTGG AGGCCATGT.

Whole-cell lysates and solubilized membrane fractions. To prepare whole-cell lysates from the testis, chilled buffer A (50 mM Tris-HCl buffer [pH 7.5], 1 mM EDTA, 0.25 M sucrose, and a protease inhibitor cocktail [Complete Mini; Roche Diagnostics]) was added to the testis (about 10 ml per g testis) and homogenized twice with a Polytron PT 3100 system (Kinematica) at 5,000 rpm for 30 s. After an equal volume of buffer A was added, the mixture was centrifuged at 800 × *g* for 10 min, and ComplexioLyte 47 (CL47; Logopharm) was added to the supernatant at a ratio of 3:1. For sperm homogenates, sperm were collected from the cauda epididymis of 2- to 6-month-old mice, solubilized by incubation in CL47 for 2 h at 4°C, and centrifuged at 20,000 × *g* for 15 min to remove nuclei.

Solubilized membrane fractions were prepared as described previ-

ously (24). In brief, tissues in buffer A were homogenized 2 to 6 times using a Polytron system as described above and were successively centrifuged at 4°C at 800 × *g* for 10 min and at 100,000 × *g* for 60 min. The precipitates were solubilized by incubation for 2 h in CL47 at 4°C, and debris was removed by centrifugation at 20,000 × *g* for 15 min. The protein concentration was determined with a Pierce bicinchoninic acid (BCA) protein assay kit (Thermo Fisher Scientific).

BN-PAGE, SDS-PAGE, and Western blotting. Blue native PAGE (BN-PAGE) (29) was performed with a NativePAGE Novex Bis-Tris gel system (Life Technologies). In brief, samples were mixed with a one-third volume of 4× NativePAGE sample buffer and 5% G-250 sample additive and were separated by electrophoresis on NativePAGE Novex 4% to 16% Bis-Tris gels. Proteins were transferred to a polyvinylidene difluoride (PVDF) membrane (Merck Millipore) and fixed in 8% acetic acid for 15 min. For SDS-PAGE, samples in SDS sample buffer (62.5 mM Tris-HCl [pH 6.8], 2% SDS, 10% glycerol, 5% β-mercaptoethanol, 0.01% bromophenol blue) were separated by electrophoresis on a 7.5% or 10% polyacrylamide gel and transferred to a PVDF membrane. For Western blotting, PVDF membranes were incubated in blocking buffer (TBS containing 10% skim milk and 0.01% Tween 20) at room temperature for 1 h and incubated at 4°C overnight with primary antibodies in Can Get Signal Solution 1 (Toyobo Life Science) or blocking buffer. The membranes were then incubated at room temperature for 1 h with secondary antibodies in Can Get Signal Solution 2 or blocking buffer, and the target protein was visualized with Immobilon Western chemiluminescent HRP substrate (Merck Millipore).

Density-gradient fractionation. Mouse C2C12 cells were infected with a retrovirus carrying cDNA for C-terminally Flag-tagged TMEM16E. The transformants (7.0×10^5) were suspended in 500 μl of 20 mM Tris-HCl buffer (pH 7.5) containing 5 mM $MgCl_2$, 5 mM $CaCl_2$, and a protease inhibitor cocktail and then homogenized on ice in a Dounce homogenizer with a tightly fitting pestle and passed through a 25-gauge needle. Unbroken cells were removed by centrifugation, and the homogenates were centrifuged at 100,000 × *g* at 4°C for 3 h through 4.4 ml of 0% to 30% OptiPrep (Alere Technologies). Fractions (0.5 ml each) were collected from the top and analyzed by SDS-PAGE followed by Western blotting.

For skeletal muscle analyses, mouse skeletal muscle (250 mg) was homogenized using a Polytron homogenizer and 5 ml of buffer B (20 mM Tris-HCl buffer [pH 7.5] containing 0.3 M sucrose) with a protease inhibitor cocktail. The homogenates were centrifuged at 800 × *g* for 10 min at 4°C, and the membrane fraction was collected by centrifugation at 20,000 × *g* for 30 min. The precipitates were suspended in buffer B and analyzed by density gradient fractionation using 0% to 30% OptiPrep as described above. Samples from each fraction were diluted by adding 1.5 volumes of buffer B and spun at 100,000 × *g* at 4°C for 1 h. Precipitates were dissolved in 150 μl of CL47 containing a protease inhibitor cocktail, rotated overnight at 4°C, subjected to BN-PAGE, and analyzed by Western blotting.

Separation of mouse sperm into heads and tails. Sperm from the cauda epididymis of 2- to 6-month-old mice were collected into cold phosphate-buffered saline (PBS) (250 μl/epididymis). Heads and tails of sperm were separated by mild sonication followed by Percoll density gradient centrifugation essentially as described previously (30). In brief, 2×10^7 sperm in 500 μl of PBS were subjected 15 times at 4°C to a 1-s flash of sonication at output level 1 using ultrasonic disrupters (UR-20P; Tomy Seiko). Samples were layered on 90% (vol/vol) Percoll (GE Healthcare) in Tris-buffered saline (TBS; 25 mM Tris-HCl [pH 7.5], 150 mM NaCl) and centrifuged at 15,000 × *g* for 15 min at 4°C. Sperm heads in the pellet and tails at the interphase were collected, diluted 5-fold with TBS, and centrifuged at 9,000 × *g* for 5 min. The precipitates were suspended in 200 μl of CL47 containing a cocktail of protease inhibitors and incubated at 4°C for 2 h. Alternatively, the precipitates were suspended in 200 μl of SDS sample buffer and heated at 85°C for 30 min. After cell debris was removed by centrifugation, the supernatant was subjected to SDS-PAGE.

Mass spectrometry. The cell lysates from tibialis anterior muscle were subjected to iodixanol density gradient centrifugation as described above. Proteins were dissolved in SDS sample buffer, incubated at room temperature for 30 min, separated by 7.5% SDS-PAGE, and stained with Pierce Silver Stain for mass spectrometry (MS; Thermo Fisher Scientific). MS analysis was carried out using a TripleTOF 5600+ system (AB Sciex) and ProteinPilot software at Kyoto University Medical Research Support Center.

PtdSer exposure. Phosphatidylserine (PtdSer) exposure on the cell surface of Ba/F3 cells was assayed as described previously (17). In brief, 10^5 cells in early exponential phase were washed twice in annexin V binding buffer (10 mM HEPES-NaOH [pH 7.4], 140 mM NaCl, 1 mM $CaCl_2$), suspended in 1 ml of annexin V binding buffer containing 5 μg/ml propidium iodide (PI) and Cy5-annexin V (Biovision; diluted 1,000-fold), and incubated for 5 min at 20°C. A Ca^{2+} ionophore, A23187 (Sigma-Aldrich), was added to the mixture to achieve a final concentration of 3 μM. Annexin V-positive cells in the PI-negative population were analyzed by FACSAria II at 20°C for 4 min.

To detect PtdSer in sperm, a D89E mutant of mouse milk fat globule epidermal growth factor 8 (D89E) was produced and purified as described previously (31) and labeled with an Alexa Fluor 647 protein labeling kit (Thermo Fisher Scientific). Sperm were incubated in TYH medium (119.37 mM NaCl, 4.78 mM KCl, 1.19 mM $MgSO_4$, 1.19 mM KH_2PO_4, 25.07 mM $NaHCO_3$, 1.71 mM $CaCl_2$, 5.56 mM D-glucose, 1 mM sodium pyruvate, 4 mg/ml AlbuMAX I [Gibco]) (32) containing 1.25 μg/ml Alexa Fluor 647-conjugated D89E at 37°C for 10 min. The sperm were then transferred to TYH medium containing 1% methylcellulose in a 35-mm-diameter glass dish, centrifuged at 500 × *g* for 3 min, and observed by confocal microscope (FV-1000D; Olympus).

Histological analysis and serum creatine kinase. Testis was fixed overnight at 4°C in PBS containing 4% paraformaldehyde (PFA), successively incubated at 4°C overnight in PBS containing 25% and 30% sucrose, embedded in Tissue-Tek OCT compound (Sakura-Finetek), and frozen in isopentane in liquid nitrogen. Tissues were sectioned at 10 μm with a cryostat (CM3050S; Leika Microsystems), fixed on APS (amino silane)-coated glass slides (Matsunami Glass), and stained with hematoxylin and eosin. The sections were dipped 10 times each in distilled water, 70% ethanol, and 80% ethanol and were dehydrated once in 90% ethanol and twice in absolute ethanol. The sections were incubated 3 times in xylene for 2 min, air dried, mounted with Mount-Quick (Daido Sangyo), and observed with a microscope (Biorevo BZ-9000; Keyence). For skeletal muscles, the tibialis anterior muscle was frozen in isopentane. Cryosections (10 μm) were fixed in 4% PFA for 5 min at room temperature and stained with hematoxylin and eosin.

For serum creatine kinase, blood collected from 7- to 10-month-old mice was left overnight at 4°C, and the serum was recovered by centrifugation at 6,000 rpm for 5 min. The creatine kinase was quantified as a custom service at Oriental Yeast.

ATP content, mitochondrial activity, and tyrosine phosphorylation. Sperm (1.5×10^6 to 3.0×10^6) were boiled for 2 min in 100 μl of boiling extraction buffer (0.1 M Tris-HCl [pH 7.8], 4 mM EDTA). After the debris was removed by centrifugation at 20,000 × *g* for 5 min, the ATP concentration was measured as described previously (33). In brief, the sample was incubated with 0.5 μg/ml firefly luciferase and 50 μg/ml luciferin in a reaction mixture containing 15.8 mM Tricine, 0.3 mM EDTA, 0.34 mM Na_3PO_4, 10.3 mM $MgSO_4$, 0.9 mM Triton X-100, 4.4 mM dithiothreitol (DTT), and 0.27 mM coenzyme A. The bioluminescence was measured by the use of a microplate reader (Infinite M200; Tecan). For mitochondrial activity analyses, sperm were incubated at 37°C for 20 min with 1.0 μM JC-1 (Thermo Fisher Scientific) in TYH medium (34) and observed by confocal microscopy. To detect the tyrosine phosphorylation of sperm proteins, sperm were suspended in SDS sample buffer without β-mercaptoethanol and heated at 96°C for 5 min. After debris was removed by centrifugation at 13,000 rpm at 4°C for 15 min, the supernatant

was separated by SDS-PAGE, followed by Western blotting with HRP-conjugated antiphosphotyrosine MAb.

Fertility, sperm motility, and flagellar trajectory. To assess fertility, 12-week-old male mice were mated for 2 months with 12-week-old wild-type female mice (one male crossed with two female mice). The pregnant female mice were separated from the other mice 3 to 5 days before delivery, and the number of pups was counted on the day of delivery.

To assess sperm motility, sperm in TYH medium at 37°C were allowed to swim out from cauda epididymis for 10 min or 120 min and were placed on standard count 2-chamber slides (Leja) (depth, 100 μm) that had been preheated to 37°C. Sperm motility parameters (curvilinear velocity [VCL], straight-line velocity [VSL], and average path velocity [VAP]) were evaluated by a computer-assisted system (HTM-CEROS version 12.3; Hamilton Thorne). The straightness of the sperm trajectory was calculated by the following formula: (VSL/VAP) × 100. Sperm that satisfied the criteria of VAP values of >50 μm/s and straightness values of >50% were classified as having progressive motility.

Sperm flagellar movement was examined as described previously (35). Briefly, sperm in TYH medium were placed on a glass chamber slide (Leja) (depth, 20 μm), and their motion was observed with an Olympus BX-53 microscope equipped with a high-speed camera (HAS-L1; Ditect). Flagellar movement was recorded at 200 frames per s, and 10 fields were observed for each sample in triplicate. Sperm flagellar waveform and frequency were analyzed using sperm motion-analyzing software (Boh-Bohsoft).

***In vitro* fertilization.** Sperm were placed in a 100-μl drop of TYH medium, covered with paraffin oil (Nacalai Tesque), and incubated at 37°C for 2 h. Eight-week-old B6D2F1 female mice were injected with 5 IU of pregnant mare serum gonadotropin 62 h before *in vitro* fertilization (IVF) and with 5 IU of human chorionic gonadotropin 14 h before IVF. Eggs were collected from the oviduct. In some cases, eggs were treated with 330 μg/ml hyaluronidase (Sigma-Aldrich) or 1 mg/ml collagenase (Sigma-Aldrich) at 37°C for 10 min to prepare cumulus-free or zona-free eggs, respectively. The eggs (50 to 60 cumulus-intact eggs, 25 to 30 cumulus-free eggs, or 10 to 20 zona-free eggs) were placed in a 100-μl TYH drop. The eggs were incubated with 2.0×10^5 sperm for 6 h at 37°C, washed with TYH medium, further incubated for 18 h, and observed using a Hoffman modulation contrast microscope (IX71; Olympus). To assay the ability of sperm to bind the zona pellucida layer, sperm (2.5×10^5) were incubated at 37°C for 30 min with 10 cumulus-free eggs in 100 μl of TYH medium, fixed with 0.1% PFA, and observed by the use of an Olympus IX-71 microscope.

Treadmill exercise test. Mice at 2 months of age were acclimatized for 2 days to the environment by running on a horizontal treadmill (TM-MV1; Osaka Microsystem) at 10 m/min for 10 min. The endurance test was started at 10 m/min for 10 min, and then the speed was incrementally increased by 3 m/min every 3 min to 22 m/min. Once the speed reached to 22 m/min, the mice were forced to run until they were exhausted. The criterion of exhaustion was that the mice stayed on electric shock bars at the bottom of treadmill for more than 10 s. The exercising period was recorded from the time when the speed reached to 22 m/min to the time when the mice were exhausted.

RESULTS

TMEM16E cellular localization. TMEM16E is strongly expressed in mouse muscle and bone (4). To examine its cellular distribution, mouse myoblast C2C12 cells (36) were transformed with Flag-tagged mouse TMEM16E. Cellular organelles were separated from extracts of the transformed cells by iodixanol-base density gradient centrifugation (37). Each gradient fraction was then separated by SDS-PAGE and analyzed by Western blotting, which revealed that the exogenously expressed Flag-tagged TMEM16E of about 106 kDa cofractionated with calnexin at the endoplasmic reticulum (ER) (38) but not with Golgin97 in the Golgi apparatus (39) (Fig. 1A).

To examine the cellular distribution of the endogenous TMEM16E, muscle extracts were separated by SDS-PAGE and analyzed by Western blotting using a hamster anti-mouse TMEM16E MAb that we prepared. However, the presence of a large amount of protein with a molecular size (about 100 kDa) similar to that of TMEM16E hampered this analysis (Fig. 1B). The tandem mass spectrometry (MS/MS) analysis of the 100-kDa protein band revealed that it was sarcoplasmic reticulum Ca^{2+}-ATPase 1 (SERCA1) (Fig. 1C). To overcome this problem, membrane fractions were separated from skeletal muscles by density gradient centrifugation, and the proteins in each fraction were solubilized and subjected to BN-PAGE (29). Western blotting with the anti-TMEM16E MAb showed that TMEM16E behaved as a protein of 540 kDa and cofractionated with calnexin (Fig. 1D), suggesting that the endogenous mouse TMEM16E localizes to the ER.

The TMEM16E scrambling domain. Among the TMEM16 family proteins, TMEM16E shares the highest homology with TMEM16F (46.4% amino acid sequence identity), and yet it lacks TMEM16F's ability to support Ca^{2+}-dependent phospholipid scrambling on the plasma membrane (6). This absence of scrambling ability is partly due to TMEM16E's intracellular localization. Recently, Yu et al. (18) showed that inserting the SCRD from mouse TMEM16F into TMEM16A, which has no scrambling ability, is sufficient to confer scramblase activity. TMEM16F's SCRD spans 35 amino acids in the region from transmembrane IV to transmembrane V. The amino acid sequences of TMEM16A, -16B, -16E, and -16F at this region are aligned in Fig. 2A, showing that 10 and 7 amino acids in this domain are identical or homologous among these four members. TMEM16E has an additional 7 amino acids (E525, K526, E542, S546, M551, F554, and Q555) that are identical or similar to TMEM16F. Ten residues were specifically conserved between TMEM16A and -16B, both of which have Cl^--channel activity. Among these 10 residues, only three amino acids (W530, K533, and M534) were found in TMEM16E (Fig. 2A). These results suggested that this segment of TMEM16E might work as a SCRD. To examine this possibility, we replaced the DNA fragment coding this segment in TMEM16A with the corresponding region of TMEM16E or -16F, generating TMEM16A-E SCRD and TMEM16A-F SCRD (Fig. 2B). TMEM16A, -16E, -16F, and the chimeric TMEM16A-E SCRD and TMEM16A-F SCRD proteins were fused to EGFP and stably expressed in 293T cells. Fluorescence microscopy showed that TMEM16A, TMEM16F, and TMEM16A-F SCRD localized to the plasma membrane (Fig. 2C). Regardless of whether EGFP was attached to the N or C terminus of TMEM16E, TMEM16E-EGFP was mostly found at intracellular membranes, which were stained with ER-tracker to confirm that TMEM16E localized to the ER (Fig. 2C and D). On the other hand, TMEM16A-E SCRD localized to the plasma membrane, indicating that the 35-amino-acid segment of TMEM16E did not block TMEM16A's localization to the plasma membrane.

Of the 5 TMEM16 family members (TMEM16C, -16D, -16F, -16G, and -16J) that promote Ca^{2+}-dependent phospholipid scrambling (6), mouse Ba/F3 cells expressed only TMEM16F (Fig. 3A). Accordingly, when *TMEM16F* was mutated using the CRISPR/Cas9 system (Fig. 3B), the ability of *TMEM16F*$^{-/-}$ Ba/F3 cells to expose PtdSer in response to A23187, a Ca^{2+} ionophore, was severely inhibited (Fig. 3C). Next, *TMEM16F*$^{-/-}$ Ba/F3 cells were stably transformed with TMEM16A, TMEM16E, TMEM16F,

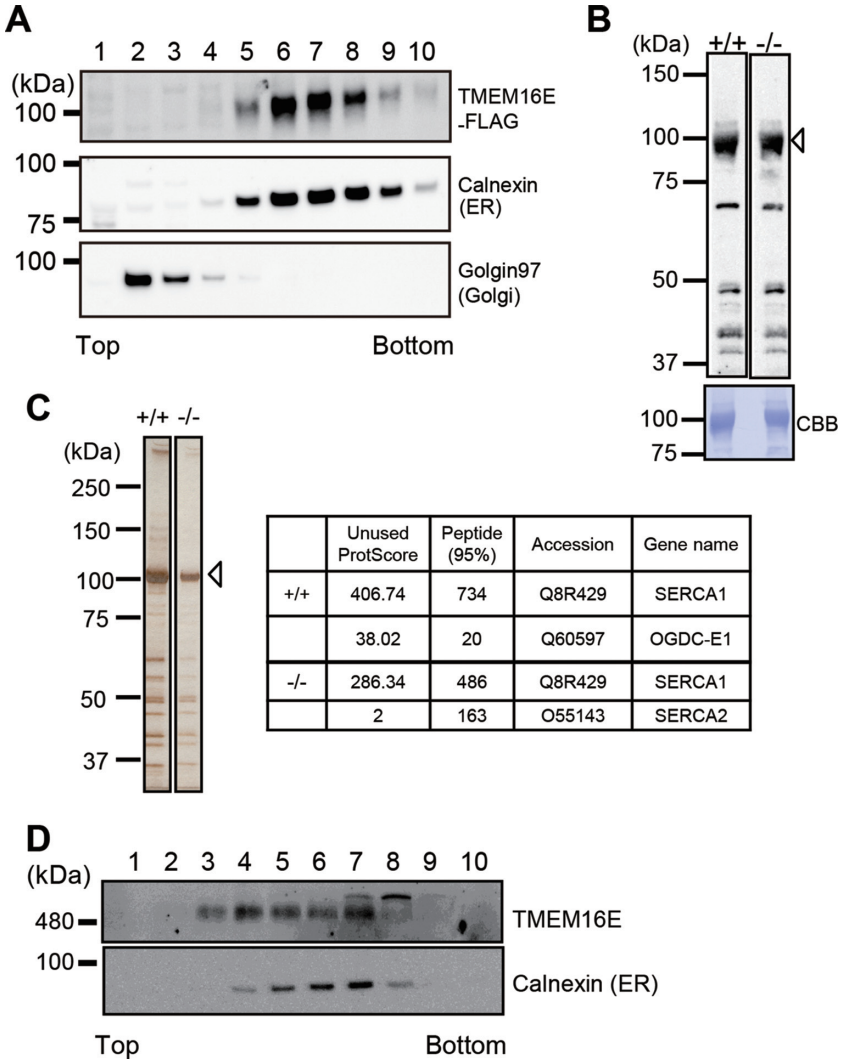

	Unused ProtScore	Peptide (95%)	Accession	Gene name
+/+	406.74	734	Q8R429	SERCA1
	38.02	20	Q60597	OGDC-E1
-/-	286.34	486	Q8R429	SERCA1
	2	163	O55143	SERCA2

FIG 1 TMEM16E's cellular localization. (A) TMEM16E in C2C12 cells. Homogenates of C2C12 cells expressing Flag-tagged mouse TMEM16E were separated by density gradient centrifugation using 0% to 30% OptiPrep, and 10-μl aliquots of each fraction were analyzed by SDS-PAGE followed by Western blotting with anti-Flag MAb, anticalnexin antibody (Ab) (endoplasmic reticulum [ER]), and anti-Golgin97 Ab (Golgi apparatus). Molecular mass standards (Precision Plus Standard; Bio-Rad) are shown on the left. (B) SDS-PAGE and Western blotting for TMEM16E in skeletal muscle. Solubilized membrane fractions (5 μg of protein) from *TMEM16E*$^{+/+}$ (+/+) and *TMEM16E*$^{-/-}$ (−/−) skeletal muscles were separated by 7.5% SDS-PAGE and analyzed by Western blotting with an anti-TMEM16E MAb. Upper panel: the nonspecific band around 100 kDa is indicated by an arrowhead. Lower panel: the membrane was stained with Coomassie brilliant blue (CBB). (C) Identification of the 100-kDa bands as SERCA1. Homogenates of skeletal muscle tissues from *TMEM16E*$^{+/+}$ and *TMEM16E*$^{-/-}$ mice were partially purified by density gradient centrifugation, separated by SDS-PAGE, and subjected to silver staining. The major band around 100 kDa (arrowhead) was analyzed by mass spectrometry (right table). Unused ProtScore, a measure of peptides that are unique to an assigned protein and that are not claimed by others. Peptide (95%), the number of distinct peptides matching a target protein sequence with at least 95% confidence. Accession, GenBank accession number. (D) TMEM16E in mouse skeletal muscle. Upper panel: homogenates from mouse skeletal muscle were analyzed by density gradient centrifugation, and 30-μl aliquots of each fraction were analyzed by BN-PAGE followed by Western blotting with anti-TMEM16E. Molecular mass standards (NativeMark unstained protein standards; Life Technologies) are shown at the left. Lower panel: aliquots of each fraction were analyzed by SDS-PAGE, followed by Western blotting with anticalnexin Abs.

TMEM16A-E SCRD, or TMEM16A-F SCRD (Fig. 3D). As previously reported (6, 18), transformants expressing TMEM16F or TMEM16A-F SCRD, but not TMEM16A or TMEM16E, exposed PtdSer in response to A23187 (Fig. 3E and F). Notably, the TMEM16A-E SCRD transformants also exposed PtdSer in response to A23187, indicating that the 35-amino-acid segment of TMEM16E worked as a SCRD. TMEM16F's ability to expose PtdSer was weaker than that of TMEM16A-E SCRD or TMEM16A-F SCRD. TMEM16F required a higher Ca^{2+} ionophore concentration than did TMEM16A-E SCRD and TMEM16A-F SCRD to expose PtdSer (data not shown), supporting the idea that TMEM16A is more sensitive than TMEM16F to Ca^{2+} (18).

***TMEM16E*-deficient mice.** We established a mouse line with floxed *TMEM16E* alleles. These mice were crossed with transgenic mice that ubiquitously expressed CRE recombinase, thereby producing *TMEM16E*$^{+/-}$ mice (Fig. 4A and B). Intercrossing *TMEM16E*$^{+/-}$ mice produced offspring at a nearly Mendelian ratio (28 *TMEM16E*$^{+/+}$, 48 *TMEM16E*$^{+/-}$, and 26 *TMEM16E*$^{-/-}$). When solubilized membrane fractions from skeletal muscles were analyzed by BN-PAGE, Western blotting with anti-TMEM16E

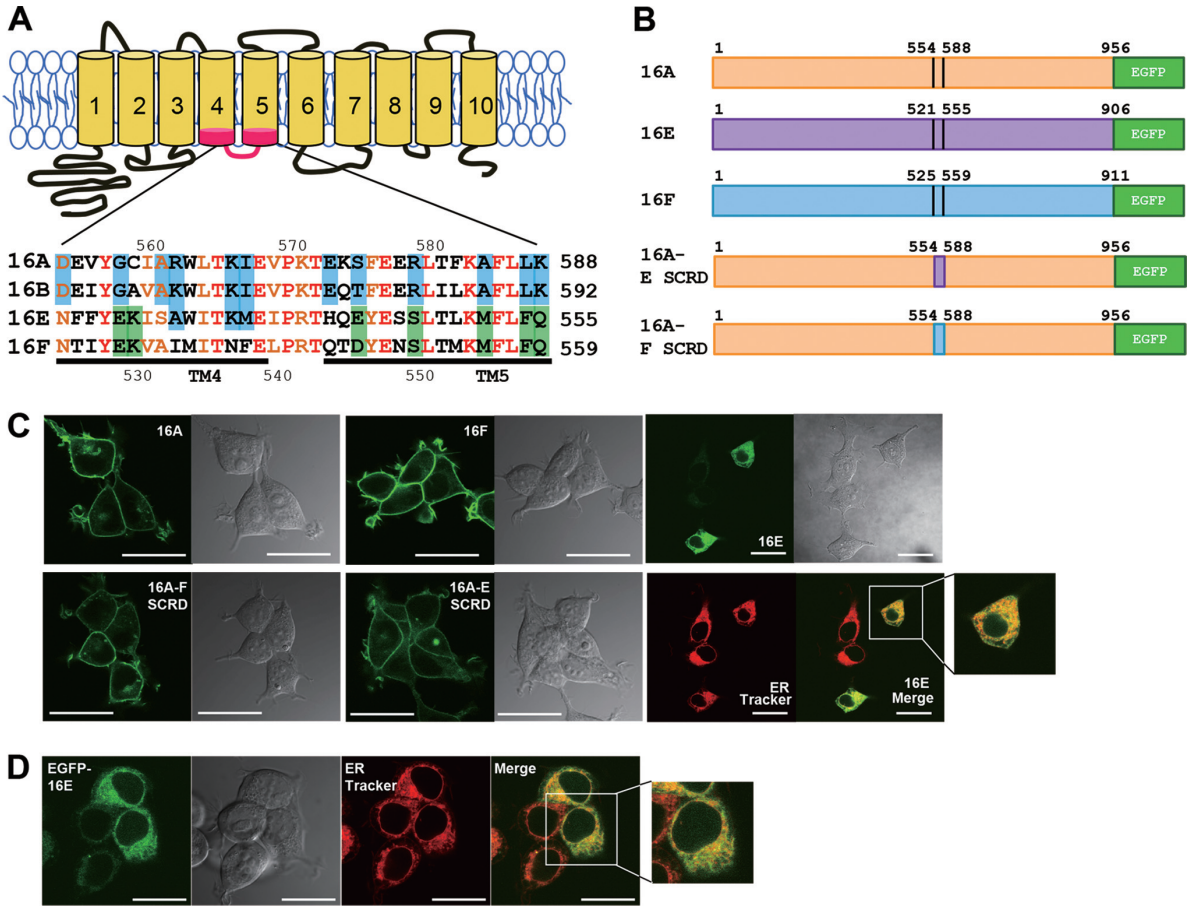

FIG 2 Chimeric TMEM16A mutants carrying the SCRD of TMEM16F or TMEM16E. (A) The putative TMEM16 SCRD. Top: schematic structure of TMEM16. The SCRD, located in the transmembrane region from IV to V in TMEM16E and -16F, is shown in pink. Bottom: amino acid sequence alignment of TMEM16A (positions 554 to 588), -16B (558 to 592), -16E (521 to 555), and -16F (525 to 559), showing identical (red) and homologous (orange) amino acids. Amino acids that were identical and homologous between TMEM16A and -16B and between TMEM16F and -16E are highlighted in blue and green, respectively. (B) A schematic representation of TMEM16A, -16E, -16F, TMEM16A-E SCRD, and TMEM16A-F SCRD. The number above each chimeric construct shows the amino acid position in TMEM16A. In the chimeric constructs, the 35-amino-acid segment in TMEM16A (positions 554 to 588) was replaced with the corresponding region of TMEM16E or -16F. TMEM16 proteins were fused to EGFP at the C terminus. (C) Stable transformants of 293T cells expressing EGFP-tagged TMEM16A, -16F, -16E, -16A-F SCRD, and -16A-E SCRD were observed by confocal microscopy. Phase-contrast and GFP images are shown. Cells expressing TMEM16E-GFP were stained with ER-tracker (ER-Tracker Blue-White DPX; Thermo Fisher Scientific), and the images were merged. Scale bars, 15 μm. (D) Stable transformants of 293T cells expressing N-terminally EGFP-tagged TMEM16E were observed by confocal microscope. Phase-contrast and GFP images are shown. The cells were also stained with ER-tracker as described above. Scale bars, 20 μm.

MAb revealed a broad band around 540 kDa in the wild-type tissues but not in the *TMEM16E*$^{-/-}$ tissues (Fig. 4C). Although human patients carrying *TMEM16E* mutations suffer from muscular dystrophy (8, 12), the skeletal muscles in the *TMEM16E*$^{-/-}$ mice, regardless of age or sex, had no apparent abnormalities (Fig. 4D and data not shown). The serum creatine kinase levels were also comparable in the *TMEM16E*$^{-/-}$ and wild-type mice (Fig. 4E). In a forced-running test, the performances of the *TMEM16E*$^{-/-}$ and wild-type mice were similar (Fig. 4F).

Subfertility in *TMEM16E*$^{-/-}$ males. *TMEM16E*$^{-/-}$ mice grew normally after birth and had no abnormalities in appearance or behavior. On the other hand, our preliminary analysis indicated that the number of offspring from crossing *TMEM16E*$^{-/-}$ mice was significantly smaller than that from wild-type mice. To determine the differences in fertility between male and female *TMEM16E*$^{-/-}$ mice, wild-type female mice were crossed with *TMEM16E*$^{+/+}$, *TMEM16E*$^{+/-}$, or *TMEM16E*$^{-/-}$ male mice and vice versa. As shown in Fig. 5A, the *TMEM16E*$^{-/-}$ and wild-type females produced similar numbers of offspring when mated with wild-type males (9.11 ± 1.26 versus 7.56 ± 1.5 pups). On the other hand, wild-type female mice crossed with *TMEM16E*$^{-/-}$ males delivered half as many pups (4.35 ± 1.86 pups) as those bred to wild-type males.

Real-time RT-PCR analysis showed higher TMEM16E mRNA levels in the testis than in skeletal muscle (Fig. 5B). BN-PAGE analysis using the anti-TMEM16E MAb detected a strong band at 720 kDa in wild-type but not *TMEM16E*$^{-/-}$ testis lysates (Fig. 5C). The difference in size between the TMEM16E proteins detected in the testes (720 kDa) and muscle (540 kDa) (Fig. 4C) suggests that TMEM16E exists as a hexamer in the testis or that TMEM16E associates with different molecules in the muscle and testis.

The testis is composed of several types of cells (germ cells, Sertoli cells, and Leydig cells). Germ cells start developing soon

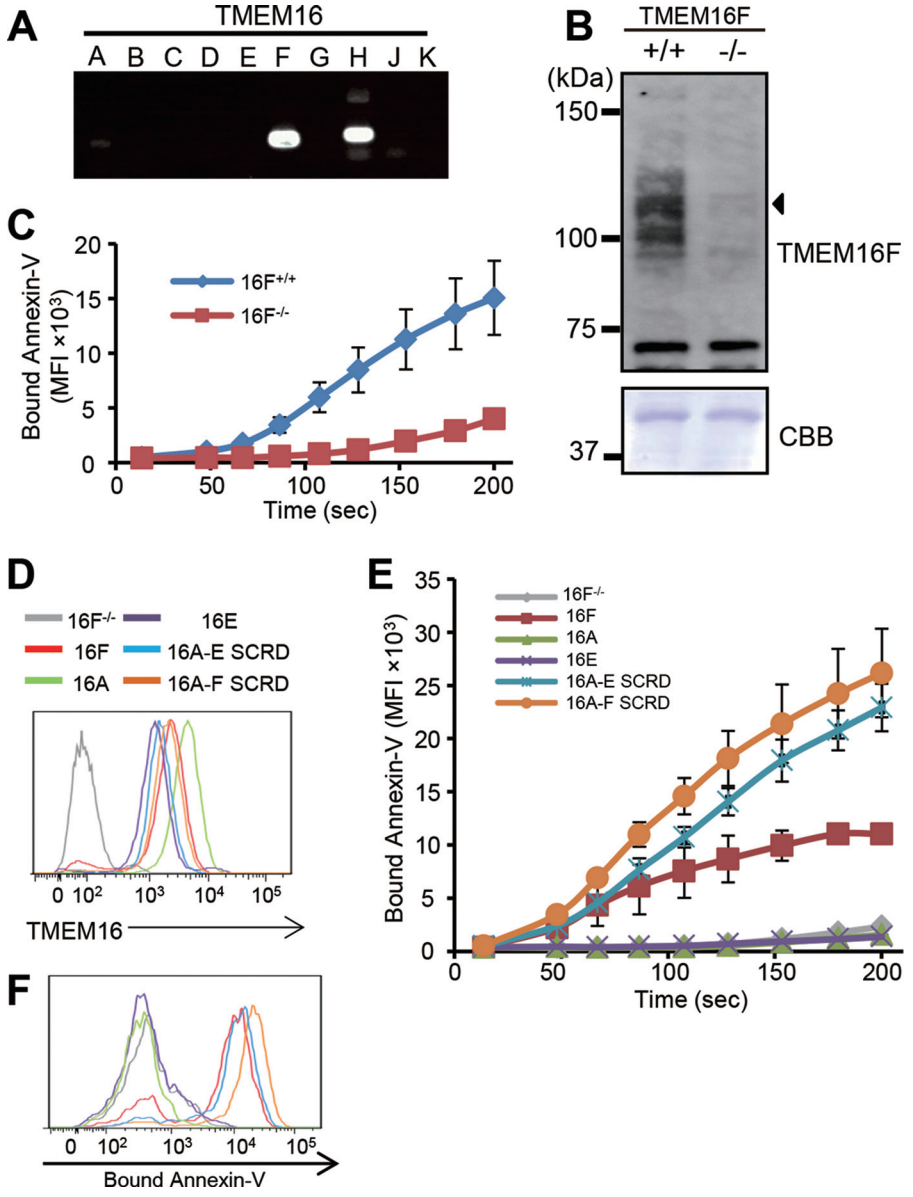

FIG 3 Phosphatidylserine scrambling by a TMEM16A chimera carrying the TMEM16E SCRD. (A) PCR of TMEM16 family members in mouse Ba/F3 cells. Total RNA from Ba/F3 cells was subjected to PCR using specific primers for the protein indicated above the lane. (B) Western blotting for TMEM16F. Whole-cell lysates (6 μg) from wild-type (+/+) and *TMEM16F*$^{-/-}$ (−/−) Ba/F3 cells were separated by SDS-PAGE and analyzed by Western blotting with an anti-TMEM16F antibody (arrowhead, TMEM16F). As a loading control, the membrane was stained with CBB. The major bands around 40 kDa are shown in the lower panel. (C) Ca^{2+}-dependent PtdSer scrambling. Wild-type and *TMEM16F*$^{-/-}$ Ba/F3 cells were treated with 3 μM A23187 at 20°C in the presence of 1 mM $CaCl_2$ and Cy5-annexin V. Cy5-annexin V staining was monitored by flow cytometry for 200 s. The results are expressed as mean fluorescence intensity (MFI) values. The average value from three experiments was plotted with standard deviations (SD). (D) EGFP-tagged TMEM16A, -16E, -16F, -16A-E SCRD, and -16A-F SCRD were expressed in *TMEM16F*$^{-/-}$ Ba/F3 cells, and EGFP in the transformants was analyzed by flow cytometry. (E and F) Ca^{2+}-dependent PtdSer scrambling by chimeric TMEM16A proteins. (E) *TMEM16F*$^{-/-}$ Ba/F3 cells and transformants expressing TMEM16A, -16E, -16F, -16A-E SCRD, or -16A-F SCRD were treated in triplicate with 3 μM A23187, and the PtdSer exposure on EGFP-expressing cells was monitored for 200 s. The average values are plotted with SD. (F) Representative histograms for the distribution of the annexin V-bound population of each transformant at 125 s are shown.

after birth (40). To determine which cell types express TMEM16E, mouse testis was collected and analyzed by BN-PAGE weekly after birth. As shown in Fig. 6A, TMEM16E was present in the testis of 2-week-old mice and its levels gradually increased thereafter, suggesting that TMEM16E expression begins in spermatocytes and is maintained in spermatozoa. Accordingly, *W/W*^{v} mice, which cannot produce differentiating germ cells due to a deficiency in a c-kit receptor that is indispensable for spermatogenesis (40), did not carry TMEM16E in the testis (Fig. 6A). Spermatozoa exit the testis to enter the epididymis, where they mature sufficiently to move toward oocytes (41). Broad bands of TMEM16E of 500 to 720 kDa were detected in mature sperm collected from the caudal epididymis (Fig. 6B). When sperm were separated into head and tail regions, higher numbers of TMEM16E were found in the basigin-positive tail region than in the SPACA1-positive head regions (Fig. 6C). Despite strong TMEM16E expression in

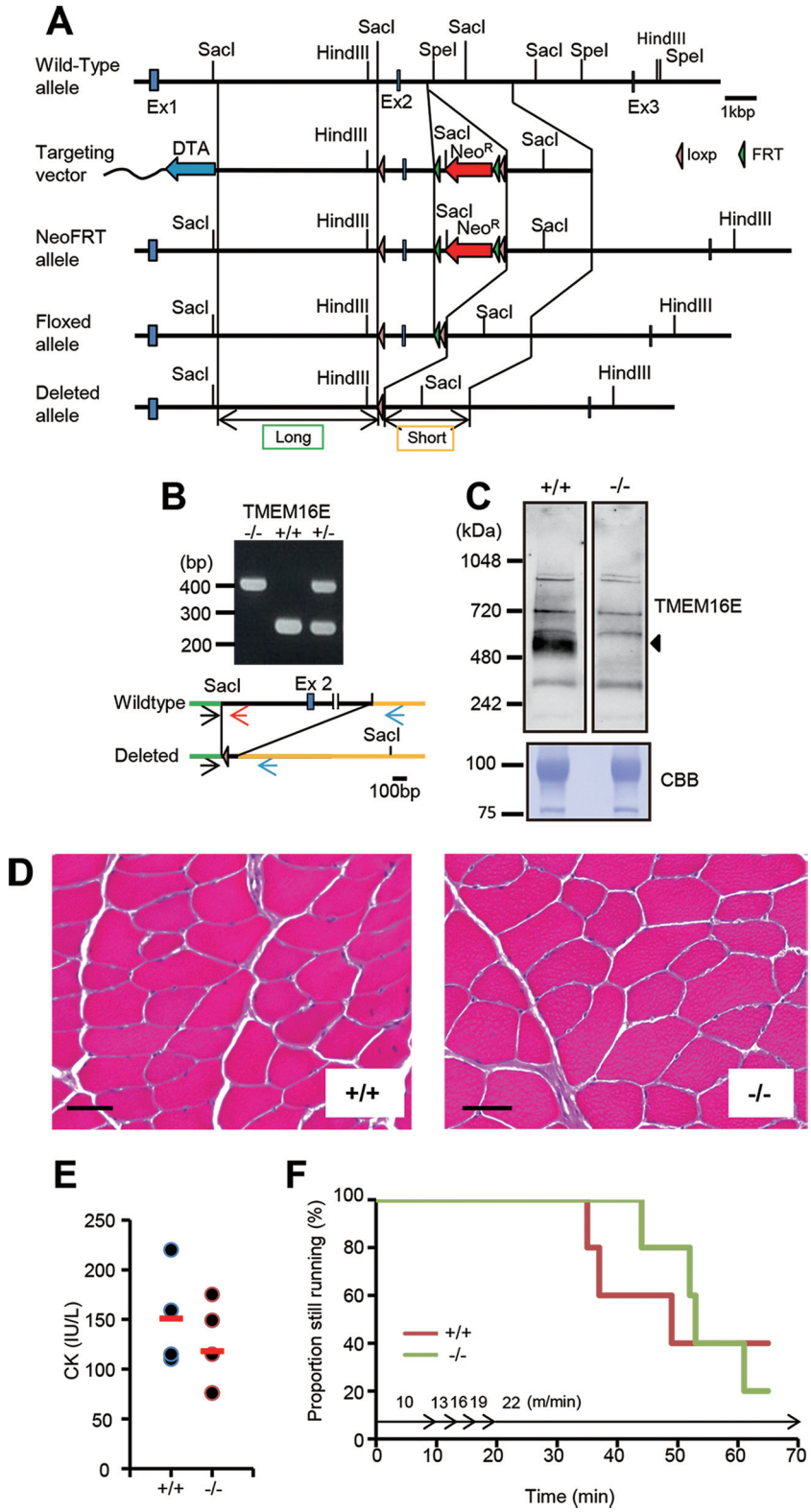

FIG 4 Generation of a *TMEM16E*-knockout mouse. (A) Schematic of wild-type and null *TMEM16E* alleles and the targeting vector, showing exons as boxes and indicating major recognition sites for restriction enzymes. The long and short arms for homologous recombination are indicated in the bottom line. In the targeting vector, exon 2 is flanked by two loxP sequences (pink arrowheads). *PGK-neo* (Neo^r) flanked by FRT sequences (green arrowheads) is inserted downstream of exon 2, and a diphtheria toxin A fragment (DTA) is at the 5′ site of the long homologous sequence. The Neo^{FRT} allele shows the allele established by homologous recombination with the targeting vector. In the floxed allele, the Neo^r gene was deleted by the use of FLPe recombinase, and exon 2 was then deleted by crossbreeding with mice carrying Cre recombinase. (B) Genotyping of the *TMEM16E*-null mice. Tail DNA from $TMEM16E^{+/+}$ (+/+), $TMEM16E^{+/-}$ (+/−), and $TMEM16E^{-/-}$ (−/−) mice was analyzed by PCR using the primers indicated in the schematic diagram at the bottom. In the diagram,

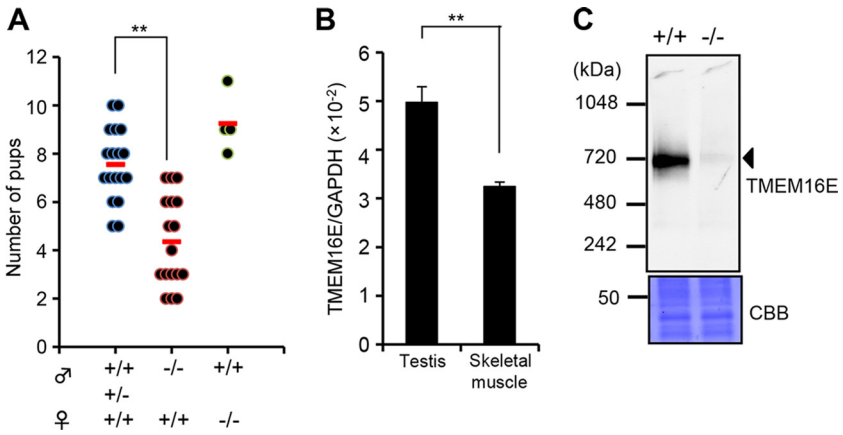

FIG 5 TMEM16E expression in mouse testis. (A) Fertility is reduced in *TMEM16E*$^{-/-}$ males. Nine males with a *TMEM16E*$^{+/+}$ (+/+) or *TMEM16E*$^{+/-}$ (+/−) genotype and 9 males with a TMEM*16E*$^{-/-}$ (−/−) genotype were mated for 2 months with *TMEM16E*$^{+/+}$ or *TMEM16E*$^{-/-}$ females. Each dot represents the number of pups born from a single breeding pair; the red line shows the average litter size. *P* values were determined by Student's *t* test. **, $P < 0.01$. (B) TMEM16E mRNA levels in the testis and skeletal muscle, measured by real-time PCR, and expressed relative to GAPDH mRNA. The values shown are averaged from 3 independent experiments and are shown with ±SD values (bars). *P* values for the different pairs were determined by the Student *t* test. **, $P < 0.01$. (C) Membrane fractions from the testis of *TMEM16E*$^{+/+}$ or *TMEM16E*$^{-/-}$ mice were solubilized, and aliquots (15 μg protein) were separated by BN-PAGE and analyzed by Western blotting with an anti-TMEM16E MAb (upper panel). The arrowhead indicates TMEM16E. Lower panel: the membrane stained with CBB.

the testis and sperm, the testis and epididymis weights were comparable in *TMEM16E*$^{-/-}$ and *TMEM16E*$^{+/+}$ mice (Fig. 6D and E), as were the numbers of sperm obtained from the caudal epididymis (Fig. 6F). The testis morphologies also appeared to be similar in the *TMEM16E*$^{+/+}$ and *TMEM16E*$^{-/-}$ mice (Fig. 6G).

Motility deficits in *TMEM16E*$^{-/-}$ sperm. The ability of *TMEM16E*$^{-/-}$ sperm to fertilize eggs was assayed *in vitro*. When cumulus-intact eggs from superovulated B6D2F1 mice were incubated with capacitated *TMEM16E*$^{+/-}$ sperm for 6 h, more than 90% of the eggs were successfully fertilized (Fig. 7A). The percentage of fertilized eggs was strongly reduced, to less than 25%, in the experiments using *TMEM16E*$^{-/-}$ sperm. The *TMEM16E*$^{-/-}$ sperm could not fertilize hyaluronidase-treated cumulus-free eggs but fully fertilized collagenase-treated zona-free eggs.

Sperm incapable of penetrating the zona pellucida often have low motility (42–44). Thus, we examined *TMEM16E*$^{-/-}$ sperm motility by incubating sperm from the caudal epididymis in TYH medium for 10 min or 2 h. The sperm motility was analyzed by a computer-assisted CEROS system. More than 95% of the *TMEM16E*$^{-/-}$ sperm could move, similarly to wild-type sperm. However, the values for all of the motility parameters (VAP [average path velocity], VSL [straight-line velocity], and VCL [curvilinear velocity]) were significantly reduced in the *TMEM16E*$^{-/-}$ sperm (Fig. 7B). The absence of TMEM16E strongly reduced the percentage of sperm that moved in a straight line, particularly after capacitation (64% versus 31%). We next plotted the VCL and straightness (an index of the departure of sperm motion from a theoretical straight line) of individual sperm. The VCL was lower in noncapacitated *TMEM16E*$^{-/-}$ sperm than in *TMEM16E*$^{+/-}$ sperm, but the straightness index in the majority of the *TMEM16E*$^{-/-}$ sperm was similar to that of *TMEM16*$^{+/-}$ sperm (Fig. 7C). Incubation in TYH medium for 2 h had little effect on the VCL but reduced the straightness of the *TMEM16E*$^{-/-}$ sperm. These results indicated that the *TMEM16E* deficiency caused sperm sluggishness, leading to inefficient *in vitro* fertilization and subfertility *in vivo*.

TMEM16E$^{-/-}$ sperm had no apparent abnormality in their morphology (Fig. 8A) and in the beating ability of flagella (Fig. 8B). They bound to the zona pellucida layer of cumulus-free eggs as efficiently as the wild-type sperm (Fig. 8C). The ATP content and mitochondrial membrane potential were also apparently normal in *TMEM16E*$^{-/-}$ sperm (Fig. 8D and E). The tyrosine phosphorylation of sperm proteins (45, 46) and the PtdSer exposure on the sperm head (47, 48) that occurred during the sperm capacitation were indistinguishable between the wild-type and *TMEM16E*$^{-/-}$ sperm (Fig. 8F and G). These results confirm that the capacitation and acrosome reaction take place normally in *TMEM16E*$^{-/-}$ sperm but that their ability to penetrate or drill into the zona pellucida layer is defective due to their sluggish motility.

green and yellow lines represent the long and short arms. Black arrows indicate the common forward primer; red and blue arrows indicate reverse primers for the wild-type and null alleles. The pink arrowhead indicates a loxP sequence. (C) BN-PAGE and Western blotting. Solubilized membrane fractions (15 μg protein) from *TMEM16E*$^{+/+}$ or *TMEM16E*$^{-/-}$ skeletal muscles were separated by BN-PAGE and analyzed by Western blotting with a hamster anti-TMEM16E MAb. A arrowhead indicates the TMEM16E band. The membrane was stained with CBB as a loading control. The major band of ~100 kDa represents SERCA. (D) *TMEM16E*$^{-/-}$ muscle had no apparent abnormalities. Cryosections of the tibialis anterior muscle from 6-month-old *TMEM16E*$^{+/+}$ and *TMEM16E*$^{-/-}$ male mice were stained with hematoxylin and eosin and observed under a microscope. Scale bar, 50 μm. (E) Serum concentration of creatine kinase (CK) in *TMEM16E*$^{+/+}$ ($n = 4$) and *TMEM16E*$^{-/-}$ ($n = 5$) male mice at 7 to 10 months of age. (F) Endurance test for *TMEM16E*$^{+/+}$ and *TMEM16E*$^{-/-}$ mice. Five mice for each genotype were subjected to the forced-running test at the speeds indicated above the *x* axis, and the percentages of mice that were still running at the indicated times were plotted.

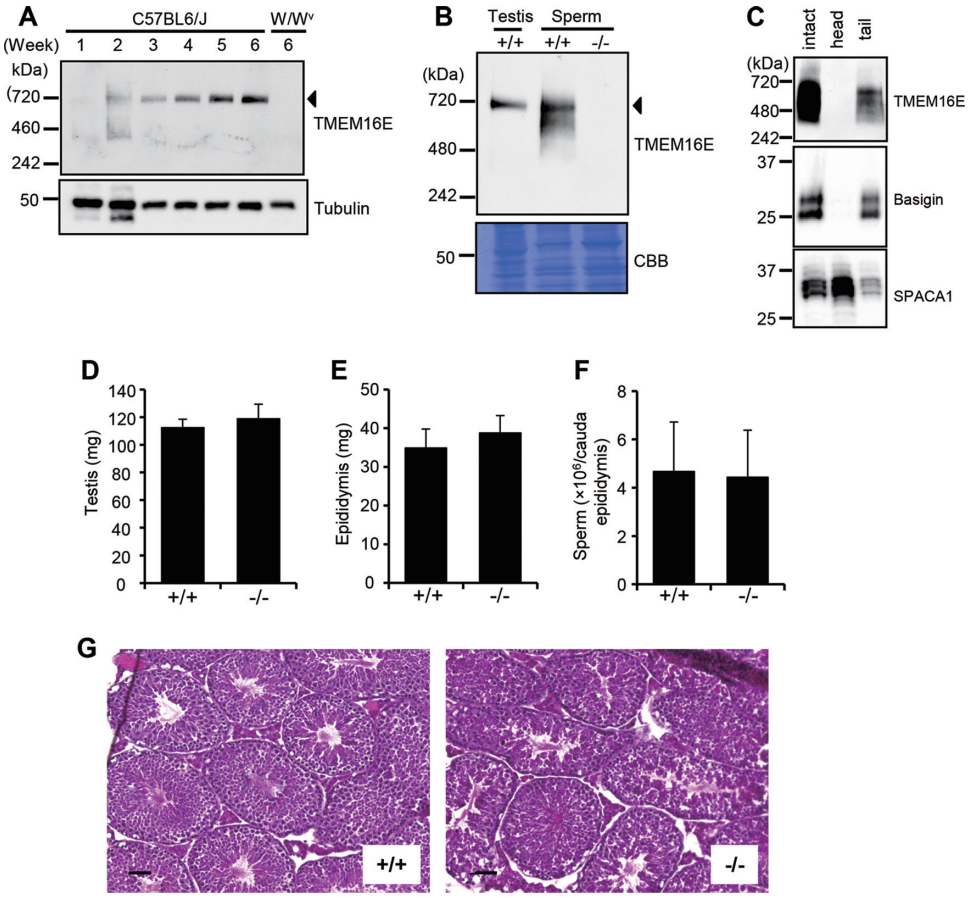

FIG 6 TMEM16E expression in mouse sperm. (A) TMEM16E in testis germ cells. Whole-cell lysates (7.5 μg protein) from the testis of C57BL6/J mice at the indicated age or from *W/W*^{v} mice at 6 weeks of age were separated by BN-PAGE and analyzed by Western blotting with an anti-TMEM16E MAb (upper panel). In the lower panel, samples (7.5 μg protein) were separated by SDS-PAGE and analyzed by Western blotting with an anti-α-tubulin MAb. The arrowhead indicates TMEM16E. (B) Whole-cell lysates from the testis or sperm of *TMEM16E*$^{+/+}$ (+/+) or *TMEM16E*$^{-/-}$ (−/−) mice were separated by BN-PAGE and analyzed by Western blotting with the anti-TMEM16E MAb (upper panel). The arrowhead indicates TMEM16E. The lower panel shows the membrane stained by CBB. (C) Localization of TMEM16E in sperm tail. Sperm (intact) were separated into head and tail. The lysates of each fraction (corresponding to 0.75×10^6 to 2×10^6 sperm) were separated by BN-PAGE and analyzed by Western blotting with anti-TMEM16E MAb. The lysates were also separated by SDS-PAGE and subjected to Western blot analysis performed with antibasigin antibody or anti-SPACA1 MAb. (D to G) No apparent abnormality in the testis and sperm of *TMEM16E*$^{-/-}$ mice. (D and E) The testis (D) and epididymis (E) were removed from wild-type and *TMEM16E*$^{-/-}$ mice at 5 to 12 months of age and were weighed. (F) Sperm were recovered from the cauda epididymis and counted. The values in panels D to F represent the average results of three experiments and are shown with SD values (bars). (G) Cryosections were prepared from the testis of 7-month-old wild-type and *TMEM16E*$^{-/-}$ mice, stained with hematoxylin and eosin, and observed under a microscope. Scale bars, 50 μm.

DISCUSSION

TMEM16A is a Ca^{2+}-dependent Cl^- channel, and TMEM16F scrambles phospholipids. Yu et al. compared the amino acid sequences in TMEM16A- and -16F paralogs (18) and showed that TMEM16F carries a specific domain (SCRD) responsible for scrambling phospholipids. Here, we applied this information to TMEM16E and found that TMEM16E also has a SCRD in the corresponding region (from transmembrane IV to transmembrane V). Our cell-based assay did not detect phospholipid-scrambling activity in TMEM16E, which localizes intracellularly (6). The amino acid residues involved in binding Ca^{2+}, inferred through a mutational analysis of mouse TMEM16A (49) and by X-ray structural analysis of *Nectria haematococca* TMEM16 (3), are well conserved in TMEM16E. Although we cannot rule out the possibility that TMEM16E lacks other domains necessary for scrambling of phospholipids, it is tempting to think that TMEM16E supports Ca^{2+}-activated phospholipid scrambling at the intracellular membrane architecture. TMEM16E is present not only in mammals but also in chickens, zebrafish, *Drosophila melanogaster*, and *Xenopus tropicalis*. As shown in Fig. 9A, TMEM16E's SCRD is phylogenetically well conserved; 18 of the 35 amino acids in the SCRD are identical or homologous among these animals. In particular, K526, E542, M551, F554, and Q555 (numbering according to mouse TMEM16E) were found in the SCRD of TMEM16E in all these animals, suggesting that TMEM16E may support phospholipid scrambling in intracellular membranes as a conserved function in various animals.

There are 10 members in the mouse TMEM16 family. Of these, not only TMEM16F but also TMEM16C, -16D, -16G, and -16J support phospholipid scrambling in a *TMEM16F*$^{-/-}$ fetal thymocyte line (6). Recently, in both *Aspergillus fumigatus* and *Nectria haematococca*, TMEM16 was shown to scramble phospholipids in a cell-free reconstituted system (3, 50). Figure 9B shows the aligned amino acid sequences of the SCRD (or its corresponding

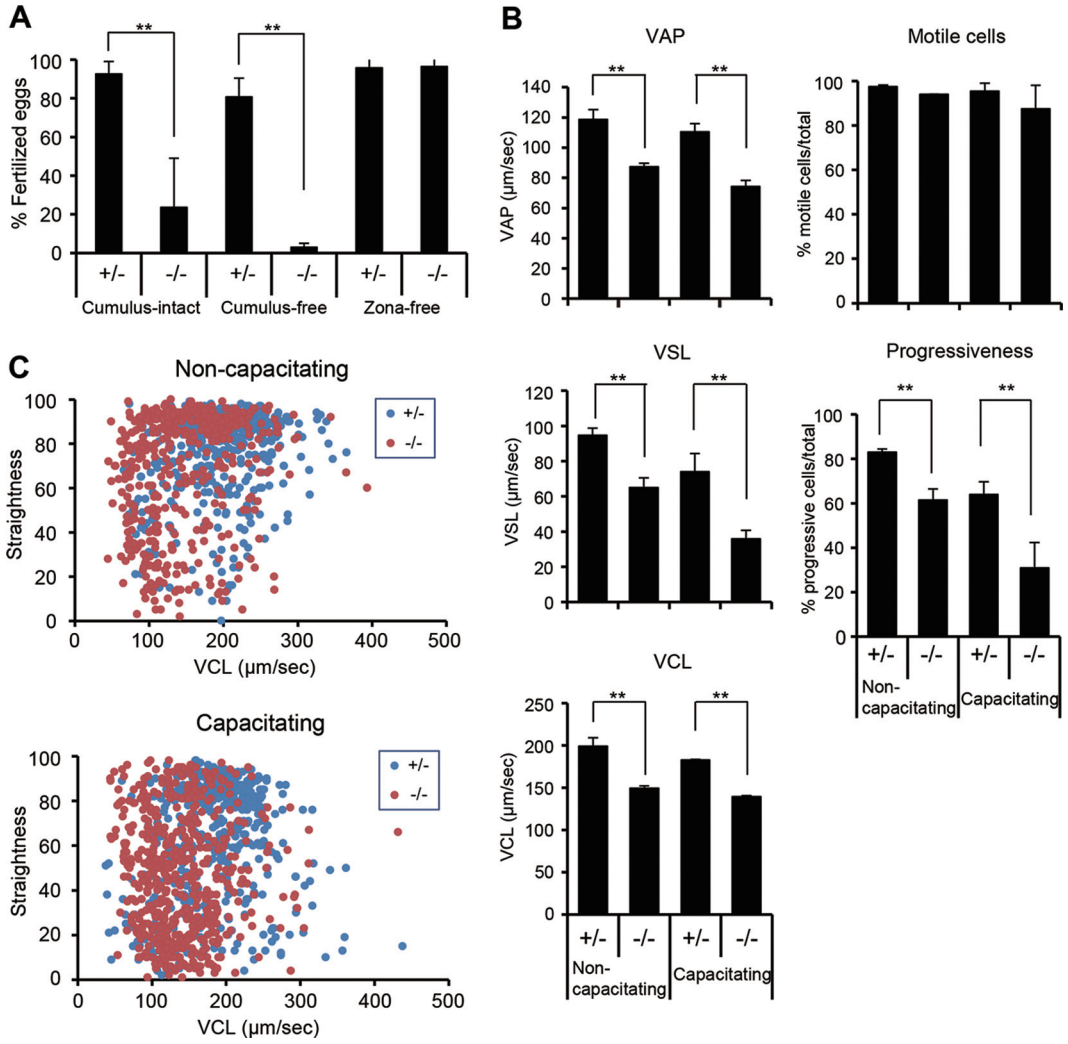

FIG 7 Reduced motility of *TMEM16E*$^{-/-}$ sperm. (A) *In vitro* fertilization. Sperm from *TMEM16E*$^{+/-}$ (+/−) or *TMEM16E*$^{-/-}$ (−/−) littermate pairs was incubated with cumulus-intact, cumulus-free, or zona-free wild-type eggs *in vitro*, and the percentages of eggs carrying pronuclei (zona-free eggs; $n = 10$ to 20) and of eggs that had reached the 2-cell stage (cumulus-intact eggs, $n = 50$ to 60; cumulus-free eggs, $n = 25$ to 30) were counted. The average values from three independent experiments are plotted and are shown with SD values (bars). *P* values were obtained by Student's *t* test. **, $P < 0.01$. (B) Sperm from three *TMEM16E*$^{+/-}$ or *TMEM16E*$^{-/-}$ mice were allowed to swim out from the dissected cauda epididymis in TYH medium for 10 min (noncapacitating) or 2 h (capacitating). The curvilinear velocity (VCL), straight-line velocity (VSL), and average path velocity (VAP) were then measured using a computer-assisted sperm analysis system. Cells with a VAP value of less than 10 μm/s were classified as immotile. Progressiveness was determined as described in Materials and Methods. The average values for each parameter were plotted with ±SD values (error bars). Student's *t* test was performed for the indicated data sets. **, $P < 0.01$. (C) Straightness of sperm movement. Noncapacitating and capacitating sperm were allowed to swim out as described for panel B. The straightness of sperm movement was assessed as described in Materials and Methods and was plotted against the VCL. Each dot represents individual sperm from two pairs of *TMEM16E*$^{+/-}$ and *TMEM16E*$^{-/-}$ mice.

region) of all mouse TMEM16 family members and of *A. fumigatus* and *N. haematococca* TMEM16. The aforementioned 7 amino acids conserved between TMEM16E and -16F (E525, K526, E542, S546, M551, F554, and Q555, with TMEM16E's numbering) were also found in the SCRD of TMEM16C and -16D. However, only a few amino acids were conserved in mouse TMEM16G and TMEM16J and in *A. fumigatus* and *N. haematococca* TMEM16. It will be interesting to examine whether these less-conserved SCRDs can confer scramblase activity in a chimeric TMEM16A molecule.

The issue of the physiological functions of TMEM16E in intracellular membranes remains. TMEM16E loss-of-function mutations cause muscular dystrophy in humans (12) (Fig. 9C) and sperm motility defects in mice (this report), while autosomal dominant mutations cause GDD (11). Although it is possible that TMEM16E performs different functions in these tissues, a common function is more likely. Phospholipids are synthesized at the cytoplasmic leaflets of the ER and are quickly flipped to the lumenal leaflet in an energy-independent mechanism (51). Although TMEM16E at the ER might be a candidate for this flipping activity, its specific expression in the muscle, bone, and testis may not support this possibility.

The clinical features of muscular dystrophy caused by a loss-of-function TMEM16E mutation(s) are similar to those of muscular dystrophy caused by defective dysferlin (52). Since dysferlin helps to repair damaged skeletal muscle membranes via a mem-

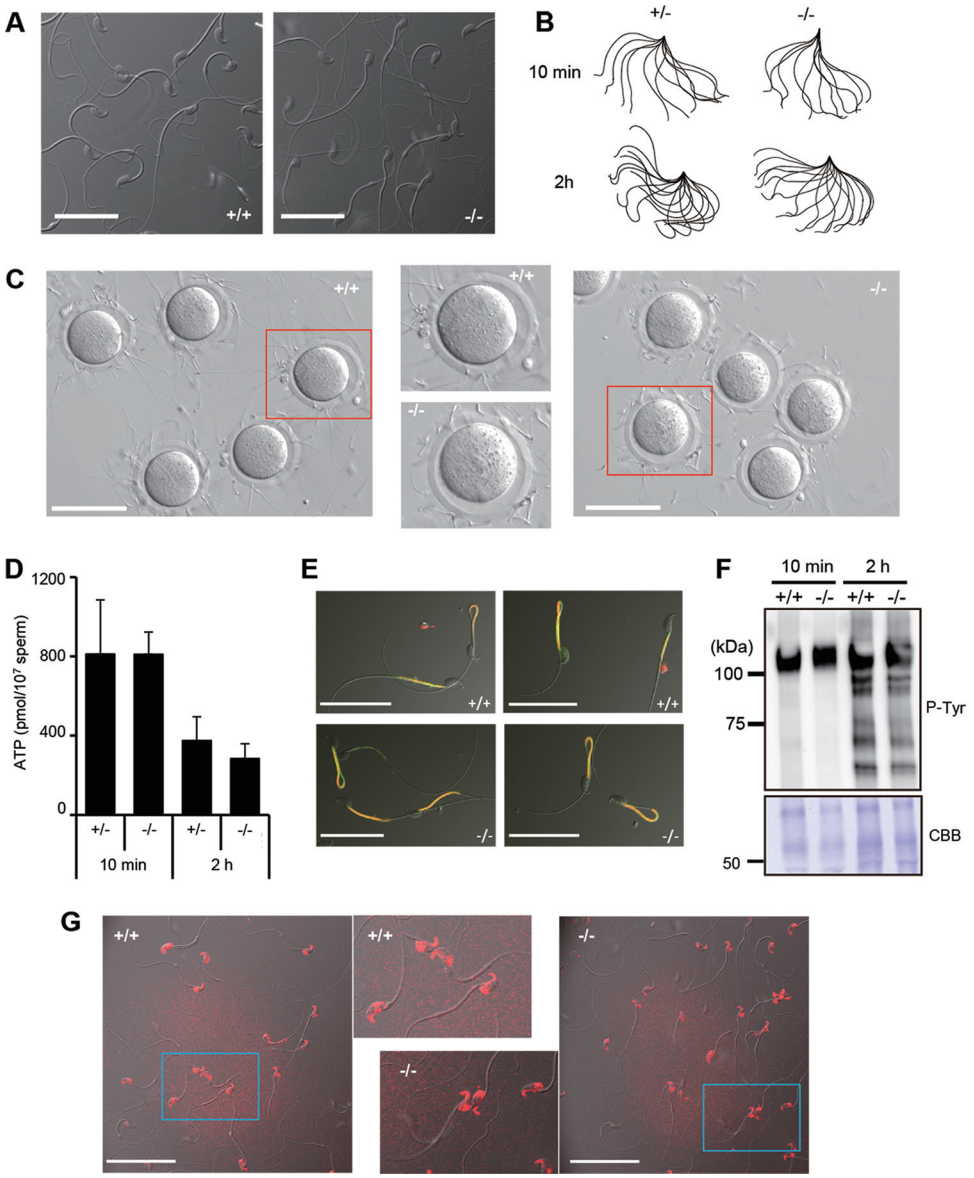

FIG 8 Morphological and functional analysis of *TMEM16E*$^{-/-}$ sperm. (A) Morphology of *TMEM16E*$^{-/-}$ sperm. Sperm were prepared from *TMEM16E*$^{+/+}$ (+/+) or *TMEM16E*$^{-/-}$ (−/−) caudal epididymis, cultured for 10 min in TYH medium, and observed under a confocal microscope. Scale bars, 30 μm. (B) Sperm flagellar movement. *TMEM16E*$^{+/-}$ or *TMEM16E*$^{-/-}$ sperm were cultured in TYH medium for 10 min or 2 h, and their movement was monitored with a high-speed camera. For each sample, 5 to 10 sperm per field were analyzed for 10 fields, and the representative movement is schematically shown. (C) Binding of sperm to zona pellucida. Cumulus-free wild-type eggs were incubated with *TMEM16E*$^{+/+}$ or *TMEM16E*$^{-/-}$ sperm that were capacitated by incubating for 2 h in TYH medium. At 30 min, the eggs were washed, fixed, and observed by confocal microscope. Eggs enclosed in a box are shown in a magnified image in the middle panels. Scale bars, 100 μm. (D) ATP content. *TMEM16E*$^{+/-}$ or *TMEM16E*$^{-/-}$ sperm were incubated for 10 min or 2 h in TYH medium, and their ATP content was quantified. Error bars indicate SD ($n = 3$ each). (E) Mitochondrial function. *TMEM16E*$^{+/+}$ or *TMEM16E*$^{-/-}$ sperm were incubated in TYH medium for 10 min, stained with 10 μM JC-1, and observed under a confocal microscope. Scale bars, 30 μm. (F) Tyrosine phosphorylation (p-Tyr) in capacitated sperm. *TMEM16E*$^{+/+}$ or *TMEM16E*$^{-/-}$ sperm were incubated for 10 min or 2 h in TYH medium. (Upper panel) The cell lysates were separated by SDS-PAGE and analyzed by Western blotting with antiphosphotyrosine MAb. In the lower panel, the membrane was stained with CBB as a loading control. (G) PtdSer exposure in sperm heads. *TMEM16E*$^{+/+}$ or *TMEM16E*$^{-/-}$ sperm were incubated in TYH medium for 10 min, stained with Alexa Fluor 647-labeled D89E, and observed under a confocal microscope. Sperm enclosed in a box are shown in magnified images in the middle panels. Scale bar, 50 μm.

brane fusion process (53), Monjaret et al. (52) proposed that TMEM16E may also be involved in repairing sarcolemmal membranes. Ferlin-1, a dysferlin homolog, functions in Ca^{2+}-dependent sperm-vesicle fusion (54). Defective ferlin-1 causes sperm infertility in *C. elegans* (55), which supports the proposal that dysferlin/ferlin and TMEM16E are involved in similar pathways. TMEM16E is expressed in both immature and mature sperm. Although we cannot rule out the possibility that TMEM16E in mature sperm regulates their motility, we prefer the hypothesis that, like ferlin-1 (54), TMEM16E affects sperm motility by regulating spermatogenesis.

There are two known plasma membrane repair mechanisms

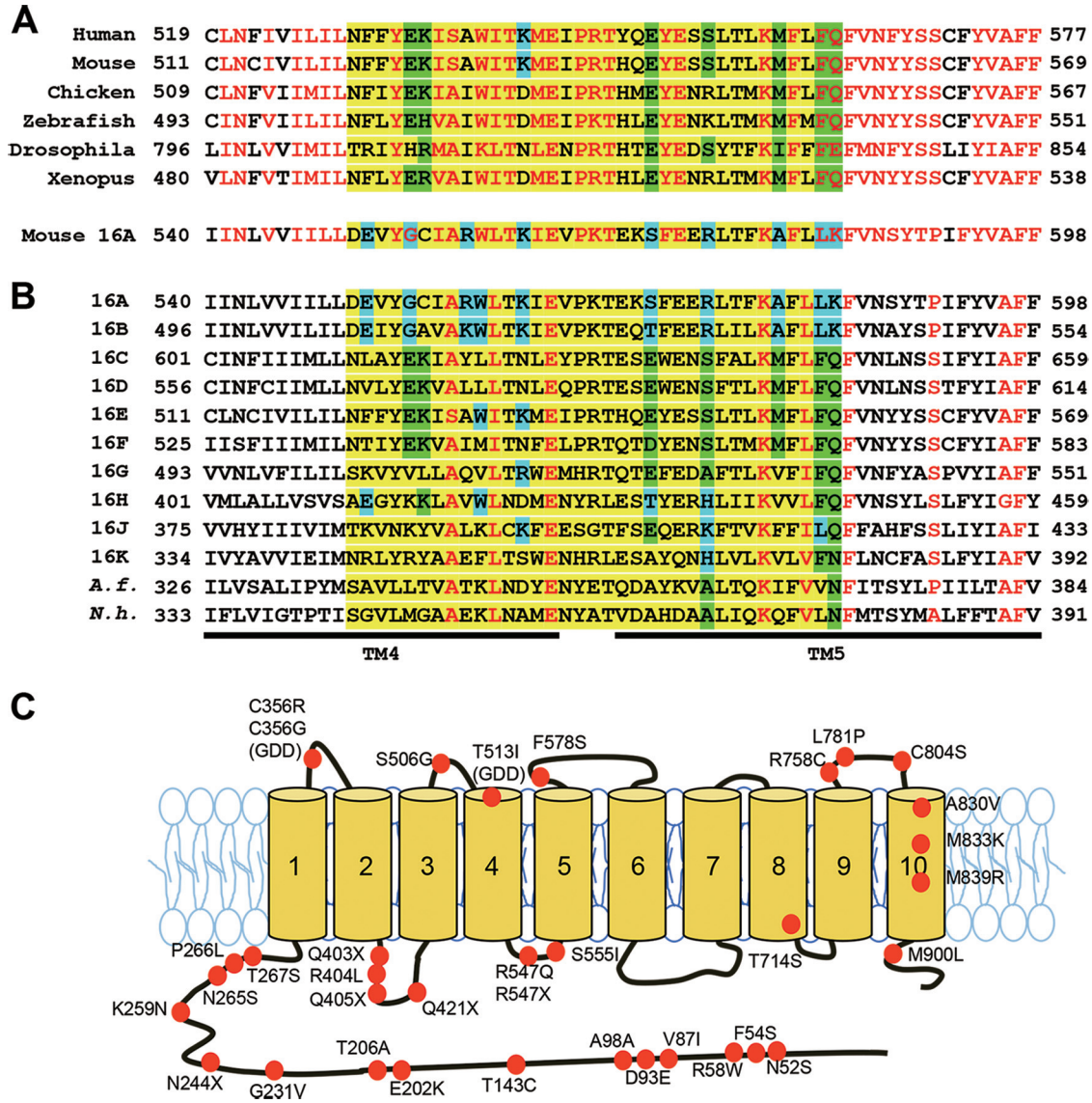

FIG 9 TMEM16E's SCRD in various animals, SCRD in mouse TMEM16 family members, and TMEM16E's mutations in human patients. (A) The sequence alignment of mouse TMEM16A amino acids in the SCRD and surrounding regions with those in TMEM16E in human, mouse, chicken, zebrafish, *Drosophila*, and *Xenopus*. (B) Sequence alignment of mouse TMEM16 family members (TMEM16A to TMEM16K) with TMEM16 from *Aspergillus fumigatus* (*A.f.*) and *Nectria haematococca* (*N.h.*), showing the SCRD (yellow highlight), amino acid residues that are conserved (i.e., that are identical or homologous) in all aligned members in each group (red), residues that are conserved specifically between mouse TMEM16A and -16B (blue), and residues that are conserved between mouse TMEM16E and -16F (green). (C) Point mutations in TMEM16E in human patients. The structure of human TMEM16E based on the tertiary structure of TMEM16 of *N. haematococca* (3) is schematically shown. Orange dots indicate the position of the point mutations in human patients with LGMD and nonspecific myopathies (12). The autosomal dominant mutations at C356 and T513 in GDD patients are also shown (7, 11).

(56). In one, the Ca^{2+}-triggered exocytosis of the damaged membrane reduces membrane tension, followed by endosomal sorting complex required for transport (ESCRT)-mediated sealing of the membrane. In the second, damaged membranes are endocytosed and degraded via the activity of multivesicular bodies (MVBs). MVBs are formed by the inward budding of limited endosomal membranes (57). We recently showed that TMEM16F, a Ca^{2+}-dependent phopholipid scramblase, is involved in the shedding of microparticles at the plasma membrane (58). TMEM16E may be involved in the budding of membranes to form multivesicular bodies, although TMEM16E mainly localizes to ER. To confirm this possibility, it would be necessary to determine whether the TMEM16A-E SCRD chimera can support microparticle production. Point mutations found in GDD patients appear to make the TMEM16E dominant-active (11, 59). It will be interesting to examine the structure of intracellular membranes in cells expressing these mutants. Loss-of-function TMEM16E mutations produce different phenotypes in humans and mice; this might be explained by differing contributions of the two membrane-repair mechanisms in human and mouse tissues. Finally, based on our findings, it will be important to investigate whether human male patients with asthenozoospermia carry TMEM16E defects.

ACKNOWLEDGMENTS

We thank Hiroshi Sakai and Atsuko Sehara-Fujisawa for the help in the analysis of mouse muscle, Shinji Ito for MS/MS analysis, and M. Fujii for secretarial assistance.

FUNDING INFORMATION

Japan Society for the Promotion of Science (JSPS) provided funding to Shigekazu Nagata. Japan Science and Technology Agency (JST) provided funding to Shigekazu Nagata.

REFERENCES

1. **Picollo A, Malvezzi M, Accardi A.** 2015. TMEM16 proteins: unknown structure and confusing functions. J Mol Biol **427:**94–105. http://dx.doi.org/10.1016/j.jmb.2014.09.028.
2. **Pedemonte N, Galietta LJV.** 2014. Structure and function of TMEM16 proteins (anoctamins). Physiol Rev **94:**419–459. http://dx.doi.org/10.1152/physrev.00039.2011.
3. **Brunner JD, Lim NK, Schenck S, Duerst A, Dutzler R.** 2014. X-ray structure of a calcium-activated TMEM16 lipid scramblase. Nature **516:**207–212. http://dx.doi.org/10.1038/nature13984.
4. **Mizuta K, Tsutsumi S, Inoue H, Sakamoto Y, Miyatake K, Miyawaki K, Noji S, Kamata N, Itakura M.** 2007. Molecular characterization of GDD1/TMEM16E, the gene product responsible for autosomal dominant gnathodiaphyseal dysplasia. Biochem Biophys Res Commun **357:**126–132. http://dx.doi.org/10.1016/j.bbrc.2007.03.108.
5. **Tsutsumi S, Inoue H, Sakamoto Y, Mizuta K, Kamata N, Itakura M.** 2005. Molecular cloning and characterization of the murine gnathodiaphyseal dysplasia gene GDD1. Biochem Biophys Res Commun **331:**1099–1106. http://dx.doi.org/10.1016/j.bbrc.2005.03.226.
6. **Suzuki J, Fujii T, Imao T, Ishihara K, Kuba H, Nagata S.** 2013. Calcium-dependent phospholipid scramblase activity of TMEM16 protein family members. J Biol Chem **288:**13305–13316. http://dx.doi.org/10.1074/jbc.M113.457937.
7. **Tsutsumi S, Kamata N, Vokes T, Maruoka Y, Nakakuki K, Enomoto S, Omura K, Amagasa T, Nagayama M, Saito-Ohara F, Inazawa J, Moritani M, Yamaoka T, Inoue H, Itakura M.** 2004. The novel gene encoding a putative transmembrane protein is mutated in gnathodiaphyseal dysplasia (GDD). Am J Hum Genet **74:**1255–1261. http://dx.doi.org/10.1086/421527.
8. **Bolduc V, Marlow G, Boycott K, Saleki K, Inoue H, Kroon J, Itakura M, Robitaille Y, Parent L, Baas F, Mizuta K, Kamata N, Richard I, Linssen W, Mahjneh I, de Visser M, Bashir R, Brais B.** 2010. Recessive mutations in the putative calcium-activated chloride channel anoctamin 5 cause proximal LGMD2L and distal MMD3 muscular dystrophies. Am J Hum Genet **86:**213–221. http://dx.doi.org/10.1016/j.ajhg.2009.12.013.
9. **Hicks D, Sarkozy A, Muelas N, Koehler K, Huebner A, Hudson G, Chinnery PF, Barresi R, Eagle M, Polvikoski T, Bailey G, Miller J, Radunovic A, Hughes PJ, Roberts R, Krause S, Walter MC, Laval SH, Straub V, Lochmüller H, Bushby K.** 2011. A founder mutation in anoctamin 5 is a major cause of limb girdle muscular dystrophy. Brain **134:**171–182.
10. **Mahjneh I, Jaiswal J, Lamminen A, Somer M, Marlow G, Kiuru-Enari S, Bashir R.** 2010. A new distal myopathy with mutation in anoctamin 5. Neuromuscul Disord **20:**791–795. http://dx.doi.org/10.1016/j.nmd.2010.07.270.
11. **Marconi C, Binello PB, Badiali G, Caci E, Cusano R, Garibaldi J, Pippucci T, Merlini A, Marchetti C, Rhoden KJ, Galietta LJV, Lalatta F, Balbi P, Seri M.** 2013. A novel missense mutation in ANO5/TMEM16E is causative for gnathodiaphyseal dyplasia in a large Italian pedigree. Eur J Hum Genet **21:**613–619.
12. **Savarese M, Di Fruscio G, Tasca G, Ruggiero L, Janssens S, De Bleecker J, Delpech M, Musumeci O, Toscano A, Angelini C, Sacconi S, Santoro L, Ricci E, Claes K, Politano L, Nigro V.** 2015. Next generation sequencing on patients with LGMD and nonspecific myopathies: findings associated with ANO5 mutations. Neuromuscul Disord **25:**533–541. http://dx.doi.org/10.1016/j.nmd.2015.03.011.
13. **Duran C, Hartzell HC.** 2011. Physiological roles and diseases of tmem16/anoctamin proteins: are they all chloride channels? Acta Pharmacol Sin **32:**685–692. http://dx.doi.org/10.1038/aps.2011.48.
14. **Yang Y, Cho H, Koo J, Tak M, Cho Y, Shim W, Park S, Lee J, Lee B, Kim B, Raouf R, Shin Y, Oh U.** 2008. TMEM16A confers receptor-activated calcium-dependent chloride conductance. Nature **455:**1210–1215. http://dx.doi.org/10.1038/nature07313.
15. **Schroeder B, Cheng T, Jan Y, Jan L.** 2008. Expression cloning of TMEM16A as a calcium-activated chloride channel subunit. Cell **134:**1019–1029. http://dx.doi.org/10.1016/j.cell.2008.09.003.
16. **Caputo A, Caci E, Ferrera L, Pedemonte N, Barsanti C, Sondo E, Pfeffer U, Ravazzolo R, Zegarra-Moran O, Galietta L.** 2008. TMEM16A, a membrane protein associated with calcium-dependent chloride channel activity. Science **322:**590–594. http://dx.doi.org/10.1126/science.1163518.
17. **Suzuki J, Umeda M, Sims PJ, Nagata S.** 2010. Calcium-dependent phospholipid scrambling by TMEM16F. Nature **468:**834–838. http://dx.doi.org/10.1038/nature09583.
18. **Yu K, Whitlock JM, Lee K, Ortlund EA, Yuan Cui Y, Hartzell HC.** 2015. Identification of a lipid scrambling domain in ANO6/TMEM16F. Elife **4:**e06901. http://dx.doi.org/10.7554/eLife.06901.
19. **Scudieri P, Caci E, Venturini A, Sondo E, Pianigiani G, Marchetti C, Ravazzolo R, Pagani F, Galietta LJV.** 2015. Ion channel and lipid scramblase activity associated with expression of tmem16F/ANO6 isoforms. J Physiol **593:**3829–3848. http://dx.doi.org/10.1113/JP270691.
20. **Suzuki J, Denning DP, Imanishi E, Horvitz HR, Nagata S.** 2013. Xk-related protein 8 and CED-8 promote phosphatidylserine exposure in apoptotic cells. Science **341:**403–406. http://dx.doi.org/10.1126/science.1236758.
21. **Sakai K, Miyazaki J-i.** 1997. A transgenic mouse line that retains Cre recombinase activity in mature oocytes irrespective of the cre transgene transmission. Biochem Biophys Res Commun **237:**318–324. http://dx.doi.org/10.1006/bbrc.1997.7111.
22. **Hanayama R, Tanaka M, Miwa K, Shinohara A, Iwamatsu A, Nagata S.** 2002. Identification of a factor that links apoptotic cells to phagocytes. Nature **417:**182–187. http://dx.doi.org/10.1038/417182a.
23. **Ray S, Diamond B.** 1994. Generation of a fusion partner to sample the repertoire of splenic B cells destined for apoptosis. Proc Natl Acad Sci U S A **91:**5548–5551. http://dx.doi.org/10.1073/pnas.91.12.5548.
24. **Fukunaga R, Ishizaka-Ikeda E, Nagata S.** 1990. Purification and characterization of the receptor for murine granulocyte colony-stimulating factor. J Biol Chem **265:**14008–14015.
25. **Fujihara Y, Satouh Y, Inoue N, Isotani A, Ikawa M, Okabe M.** 2012. SPACA1-deficient male mice are infertile with abnormally shaped sperm heads reminiscent of globozoospermia. Development **139:**3583–3589. http://dx.doi.org/10.1242/dev.081778.
26. **Morita S, Kojima T, Kitamura T.** 2000. Plat-E: an efficient and stable system for transient packaging of retroviruses. Gene Ther **7:**1063–1066. http://dx.doi.org/10.1038/sj.gt.3301206.
27. **Cong L, Ran FA, Cox D, Lin S, Barretto R, Habib N, Hsu PD, Wu X, Jiang W, Marraffini LA, Zhang F.** 2013. Multiplex genome engineering using CRISPR/Cas systems. Science **339:**819–823. http://dx.doi.org/10.1126/science.1231143.
28. **Segawa K, Kurata S, Yanagihashi Y, Brummelkamp T, Matsuda F, Nagata S.** 2014. Caspase-mediated cleavage of phospholipid flippase for apoptotic phosphatidylserine exposure. Science **344:**1164–1168. http://dx.doi.org/10.1126/science.1252809.
29. **Wittig I, Braun H-P, Schägger H.** 2006. Blue native PAGE. Nat Protoc **1:**418–428. http://dx.doi.org/10.1038/nprot.2006.62.
30. **Yamaguchi R, Yamagata K, Ikawa M, Moss SB, Okabe M.** 2006. Aberrant distribution of ADAM3 in sperm from both angiotensin-converting enzyme (Ace)- and calmegin (Clgn)-deficient mice. Biol Reprod **75:**760–766. http://dx.doi.org/10.1095/biolreprod.106.052977.
31. **Asano K, Miwa M, Miwa K, Hanayama R, Nagase H, Nagata S, Tanaka M.** 2004. Masking of phosphatidylserine inhibits apoptotic cell engulfment and induces autoantibody production in mice. J Exp Med **200:**459–467. http://dx.doi.org/10.1084/jem.20040342.
32. **Tateno H, Kamiguchi Y.** 2007. Evaluation of chromosomal risk following intracytoplasmic sperm injection in the mouse. Biol Reprod **77:**336–342. http://dx.doi.org/10.1095/biolreprod.106.057778.
33. **Chida J, Kido H.** 2014. Extraction and quantification of adenosine triphosphate in mammalian tissues and cells. Methods Mol Biol **1098:**21–32. http://dx.doi.org/10.1007/978-1-62703-718-1_2.
34. **Mukai C, Okuno M.** 2004. Glycolysis plays a major role for adenosine triphosphate supplementation in mouse sperm flagellar movement. Biol Reprod **71:**540–547. http://dx.doi.org/10.1095/biolreprod.103.026054.
35. **Miyata H, Satouh Y, Mashiko D, Muto M, Nozawa K, Shiba K, Fujihara Y, Isotani A, Inaba K, Ikawa M.** 2015. Sperm calcineurin inhibition

prevents mouse fertility with implications for male contraceptive. Science **350:**442–445. http://dx.doi.org/10.1126/science.aad0836.
36. **Yoshida S, Fujisawa-Sehara A, Taki T, Arai K, Nabeshima Y.** 1996. Lysophosphatidic acid and bFGF control different modes in proliferating myoblasts. J Cell Biol **132:**181–193. http://dx.doi.org/10.1083/jcb.132.1.181.
37. **Graham J, Ford T, Rickwood D.** 1994. The preparation of subcellular organelles from mouse liver in self-generated gradients of iodixanol. Anal Biochem **220:**367–373. http://dx.doi.org/10.1006/abio.1994.1351.
38. **Wada I, Rindress D, Cameron PH, Ou WJ, Doherty JJ, Louvard D, Bell AW, Dignard D, Thomas DY, Bergeron JJ.** 1991. SSR alpha and associated calnexin are major calcium binding proteins of the endoplasmic reticulum membrane. J Biol Chem **266:**19599–19610.
39. **Griffith KJ, Chan EK, Lung CC, Hamel JC, Guo X, Miyachi K, Fritzler MJ.** 1997. Molecular cloning of a novel 97-kd Golgi complex autoantigen associated with Sjögren's syndrome. Arthritis Rheum **40:**1693–1702. http://dx.doi.org/10.1002/art.1780400920.
40. **Mauduit C, Hamamah S, Benahmed M.** 1999. Stem cell factor/c-kit system in spermatogenesis. Hum Reprod Update **5:**535–545. http://dx.doi.org/10.1093/humupd/5.5.535.
41. **Cornwall G.** 2009. New insights into epididymal biology and function. Hum Reprod Update **15:**213–227.
42. **Ren D, Navarro B, Perez G, Jackson AC, Hsu S, Shi Q, Tilly JL, Clapham DE.** 2001. A sperm ion channel required for sperm motility and male fertility. Nature **413:**603–609. http://dx.doi.org/10.1038/35098027.
43. **Roy A, Lin YN, Agno JE, DeMayo FJ, Matzuk MM.** 2007. Absence of tektin 4 causes asthenozoospermia and subfertility in male mice. FASEB J **21:**1013–1025. http://dx.doi.org/10.1096/fj.06-7035com.
44. **Sato H, Taketomi Y, Isogai Y, Miki Y, Yamamoto K, Masuda S, Hosono T, Arata S, Ishikawa Y, Ishii T, Kobayashi T, Nakanishi H, Ikeda K, Taguchi R, Hara S, Kudo I, Murakami M.** 2010. Group III secreted phospholipase A2 regulates epididymal sperm maturation and fertility in mice. J Clin Invest **120:**1400–1414. http://dx.doi.org/10.1172/JCI40493.
45. **Leyton L, Saling P.** 1989. 95 kd sperm proteins bind ZP3 and serve as tyrosine kinase substrates in response to zona binding. Cell **57:**1123–1130. http://dx.doi.org/10.1016/0092-8674(89)90049-4.
46. **Visconti PE, Moore GD, Bailey JL, Leclerc P, Connors SA, Pan D, Olds-Clarke P, Kopf GS.** 1995. Capacitation of mouse spermatozoa. II. Protein tyrosine phosphorylation and capacitation are regulated by a cAMP-dependent pathway. Development **121:**1139–1150.
47. **Gadella BM, Harrison RA.** 2000. The capacitating agent bicarbonate induces protein kinase A-dependent changes in phospholipid transbilayer behavior in the sperm plasma membrane. Development **127:**2407–2420.
48. **Avalos-Rodríguez A, Ortíz-Muñíz AR, Ortega-Camarillo C, Vergara-Onofre M, Rosado-García A, Rosales-Torres AM.** 2004. Fluorometric study of rabbit sperm head membrane phospholipid asymmetry during capacitation and acrosome reaction using annexin-V FITC. Arch Androl **50:**273–285. http://dx.doi.org/10.1080/01485010490448741.
49. **Yu K, Duran C, Qu Z, Cui Y-y, Hartzell HC.** 2012. Explaining calcium-dependent gating of anoctamin-1 chloride channels requires a revised topology. Circ Res **110:**990–999. http://dx.doi.org/10.1161/CIRCRESAHA.112.264440.
50. **Malvezzi M, Chalat M, Janjusevic R, Picollo A, Terashima H, Menon AK, Accardi A.** 2013. Ca2+-dependent phospholipid scrambling by a reconstituted TMEM16 ion channel. Nat Commun **4:**2367.
51. **Hankins HM, Baldridge RD, Xu P, Graham TR.** 2015. Role of flippases, scramblases, and transfer proteins in phosphatidylserine subcellular distribution. Traffic **16:**35–47. http://dx.doi.org/10.1111/tra.12233.
52. **Monjaret F, Suel-Petat L, Bourg-Alibert N, Vihola A, Marchand S, Roudaut C, Gicquel E, Udd B, Richard I, Charton K.** 2013. The phenotype of dysferlin-deficient mice is not rescued by adeno-associated virus-mediated transfer of anoctamin 5. Hum Gene Ther Clin Dev **24:**65–76. http://dx.doi.org/10.1089/humc.2012.217.
53. **Han R, Campbell KP.** 2007. Dysferlin and muscle membrane repair. Curr Opin Cell Biol **19:**409–416. http://dx.doi.org/10.1016/j.ceb.2007.07.001.
54. **Washington N, Ward S.** 2006. FER-1 regulates Ca2+-mediated membrane fusion during C. elegans spermatogenesis. J Cell Sci **119:**2552–2562. http://dx.doi.org/10.1242/jcs.02980.
55. **Achanzar WE, Ward S.** 1997. A nematode gene required for sperm vesicle fusion. J Cell Sci **110:**1073–1081.
56. **Andrews NW, Almeida PE, Corrotte M.** 2014. Damage control: cellular mechanisms of plasma membrane repair. Trends Cell Biol **24:**734–742. http://dx.doi.org/10.1016/j.tcb.2014.07.008.
57. **Hanson PI, Cashikar A.** 2012. Multivesicular body morphogenesis. Annu Rev Cell Dev Biol **28:**337–362. http://dx.doi.org/10.1146/annurev-cellbio-092910-154152.
58. **Fujii T, Sakata A, Nishimura S, Eto K, Nagata S.** 2015. TMEM16F is required for phosphatidylserine exposure and microvesicle release in activated mouse platelets. Proc Nat Acad Sci U S A **112:**12800–12805. http://dx.doi.org/10.1073/pnas.1516594112.
59. **Tran TT, Tobiume K, Hirono C, Fujimoto S, Mizuta K, Kubozono K, Inoue H, Itakura M, Sugita M, Kamata N.** 2014. TMEM16E (GDD1) exhibits protein instability and distinct characteristics in chloride channel/pore forming ability. J Cell Physiol **229:**181–190. http://dx.doi.org/10.1002/jcp.24431.